Optics and Photonics Research for Montana Economic Development - MREDI Project
Quarter 4 Report – Aug. 8, 2016
Joseph A. Shaw, Principal Investigator (joseph.shaw@montana.edu)

Introduction
This project is on schedule and within budget, and is continuing to enable important collaboration between the optics and photonics research and business communities. In the following pages we report specific progress toward meeting the milestones for each subproject.

Subproject 1: Ultra-compact spectral imagers for precision agriculture and mapping of wildfires and natural resources (Joseph Shaw, joseph.shaw@montana.edu, with NWB Sensors, Inc.). Development of ultra-compact imaging systems for weed mapping in precision agriculture, UAV mapping of wildfires, and a wide variety of ground-based and airborne remote sensing.

Milestones

a) September 30, 2015: Initial agricultural data collection completed
b) December 31, 2015: Initial weed maps complete
c) June 30, 2016: Prepare a refined imaging system and application-specific algorithm
d) December 31, 2016: Complete results of summer 2016 harvest experiment
e) June 30, 2017: Finish imaging system and algorithms and transfer to private partner

Progress toward objectives

Our efforts are focused on developing compact optical sensor systems for mapping weeds for Montana agriculture and for enabling a wider variety of studies of the natural Montana environment, including forest fires and ecology. The primary tasks during this fourth quarter were devoted to preparing for field experiments for testing weed mapping during the 2016 harvest and testing airborne imaging and laser remote sensing systems for agriculture and ecology. These efforts are on schedule and within budget.

For weed mapping, our fourth-quarter activities were focused on preparing equipment for the 2016 summer harvest. We found our machine learning process to be successful with the visible light camera (GoPro) that was used during last year's harvest. Therefore, we decided to implement several different visible-light cameras during this year's harvest because of the success we had in distinguishing between the ripe grain crops and weeds during the 2015 tests. We also will collect data with an infrared imaging system again to compare results with the visible-light data. In addition to the data collection in these ripe grain fields, there has also been an opportunity to collect data in fields containing dried peas. This is a very recent and promising application for our machine learning process, which we expect to produce similar successful results.

Weed mapping

Motivated by success with visible-light cameras in 2015, we applied the additional training parameters and filters used in the visible-light data training to the near-infrared imagery. The results were successful, but the visible-light cameras (GoPros) proved to be more accurate in the end. We found that the data collected from the near-infrared imagery was very noisy during low light conditions and would produce more false positives than the visible-light cameras in the same conditions.

Figure 1 shows examples of the data processing procedures applied to the visible-light images collected during the 2015 harvest. In this figure the left four images show the output of the four detection algorithms. Blue represents low probability that a pixel is a particular object (-1) and yellow represents high probability of detection (1). The green borders are unprocessed pixels (0). The right panels represent the detection masks (after thresholds have been applied), with blue representing no detection and yellow representing a pixel where weeds have been detected. The text on the top of the left panels show a summary of the detection state. In this case, no header is detected, weeds are detected, the weed-filled pixels are not milk weeds, and the weed-filled pixels are quack grass.

Figure 2 shows examples of the near-infrared camera images processed from the 2015 harvest using the Normalized Difference Vegetation Index (NDVI) as the primary method for detecting green weeds in the midst of ripe barley or wheat. Because of the higher level of noise in these data, we were not able to do species identification.

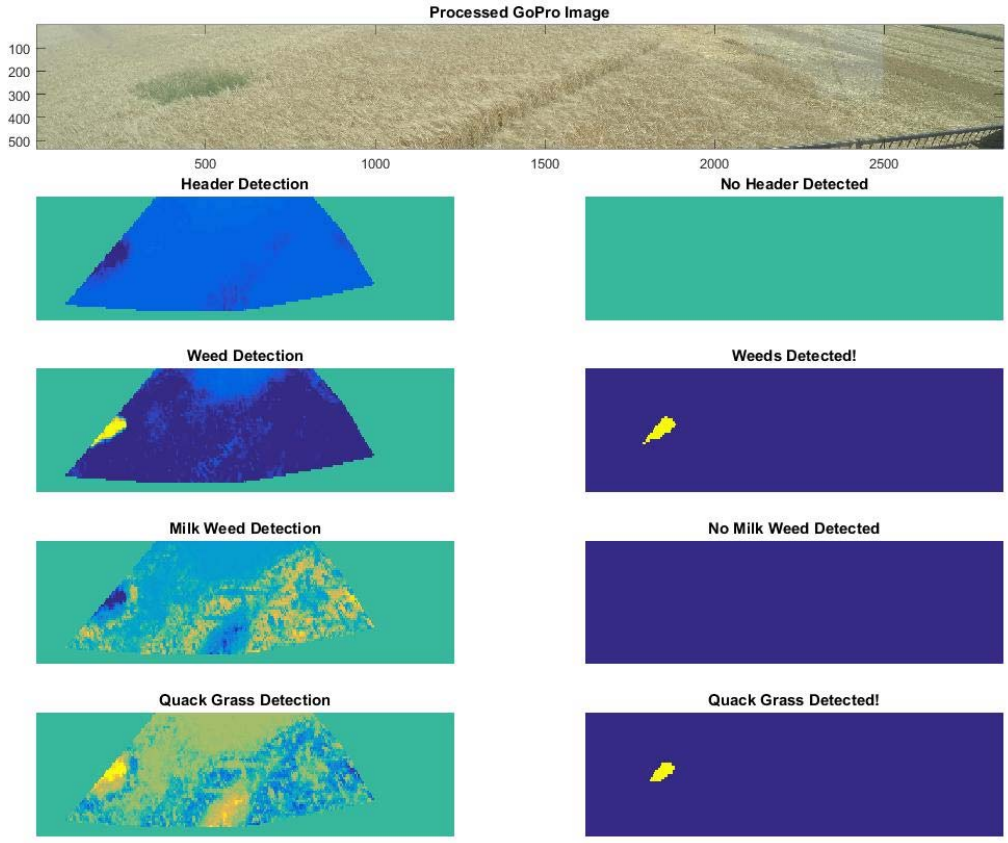

Figure 1. Processed GoPro imagery from the 2015 harvest experiments.

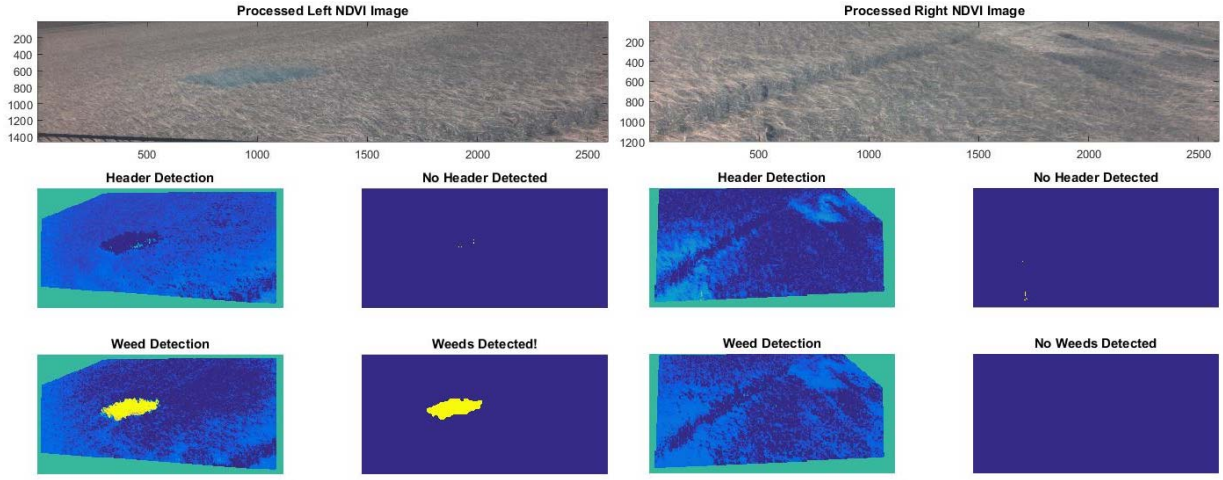

Figure 2. Processed Left and Right NDVI Imagery.

Weed Mapping System Optimization

There have been several changes to our NDVI imaging system. For example, we Improved GPS accuracy by adding a 28-dB SMA antenna to the Ultimate GPS Breakout v3 receiver. We are still using the Raspberry Pi No-IR Camera v1.3 (Raspberry Pi Camera without the infrared blocking filter). However, instead of creating a wide field of view with two of these cameras, we now include a normal Pi Camera v1.3 and the Pi No-IR Camera v1.3. These cameras will both face forward instead of the outward facing angles used in 2015. The narrower field of view will require the system to be angled slightly more toward the horizon so we can collect data within the full width of the combine header.

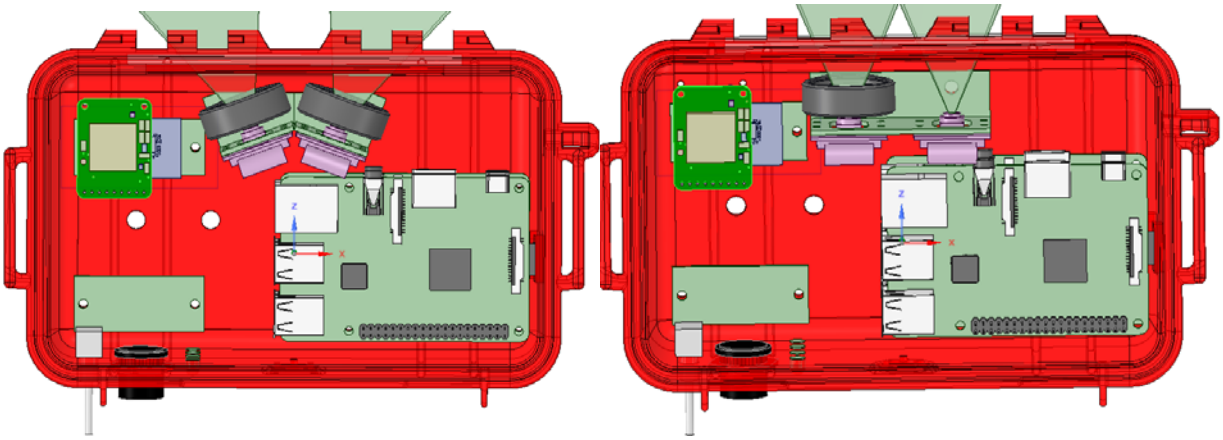

Figure 3. Old NDVI imaging system (left) and the new NDVI imaging system (right).

Another important change was to implement the higher-resolution Pi Camera v2.1 and the Pi No-IR Camera v2.1. The new Sony IMX219 8-megapixel sensor in the Pi Camera will provide higher-resolution images for the Raspberry Pi NDVI imaging system.

We also simplified the Raspberry Pi NDVI imager by removing the router from the system. To do this, we had to turn one of the two Raspberry Pis into an access point. The wireless communication between the Raspberry Pis and the ability to connect to the system for software debugging or data verification is still

intact after the removal of the router. The simplification will require less equipment to be placed in the combine during use.

A further preparation step was incorporating the correct adapters for the various power configurations inside each of the combines. The adapters will provide a more reliable way to power each of the imaging systems, thereby simplifying the cameras' use.

To increase operation time and reduce operator involvement, we bought several large-capacity, high-speed flash drives that allow the Raspberry Pi imaging systems to collect data for a couple days without interruption. There was additional modification of the camera systems to allow the farmer to easily access and change out the storage devices when they become full. We are expecting to collect much more data than we did during last year's harvest.

A magnetic mount for the Garmin camera (Fig. 4) has been developed to not obstruct the driver's view. The GPS data obtained with the Garmin camera inside a stationary combine for several hours showed that we have improved our GPS accuracy by a factor of ten (with a 5-m maximum uncertainty). The mean GPS stray during this experiment was approximately 1.4 m, while the maximum offset was 2.3 m.

Figure 4. Magnetic Mount for the Garmin Virb XE.

Weed Species Identification

An application-specific algorithm has been developed using the 2015 visible-light camera data. This allows discrimination between quack grass and milk weed, enabled by analyzing the texture differences between these two types of weeds (Fig. 5). During the 2016 harvest, we will collect data from several new crops, including dried peas, chickpeas, soy beans, and canola. In 2016 we will attempt to map invasive plants in crops containing milk thistle, cheat grass, and wild oats.

Figure 5. Texture and Color differences between Milk weed (left side) and Quack Grass (right side).

Plans for 2016 Data Collection

We have spoken with several farmers who will be willing to implement our camera systems in different regions of Montana. The majority of these farmers we have already worked with in Fairfield, MT. A new contact in Sun River Valley and a local farmer close to MSU, who also has a considerable amount of grain crops, will provide us with a more diverse data set. We are planning to implement a real-time processing system with the use of an Intel Nuc, a small portable computer powerful enough to process the images from the Garmin camera. We will work with a local farmer on this application of the system because he will be harvesting during a later time period than the crops in Fairfield.

Camera Spectral Response Measurements

During this quarter we have also been working on automating a spectral measurement process for all of the cameras that we are using during this experiment. The automated spectral measurement process will allow any camera to be characterized. We have been approached by the Space Science and Engineering Laboratory group at MSU for the ability to characterize some of their cameras as well. The automated process will provide an accurate spectral response for each camera. This process was done manually before and took a considerable amount of time.

We use several instruments to perform the necessary characterizations (Fig. 6). Using a power meter and spectrometer separately, we measured the response of a monochromator. This allowed us to characterize the response of the monochromator which can then be used alongside the measurement collected by each of the cameras.

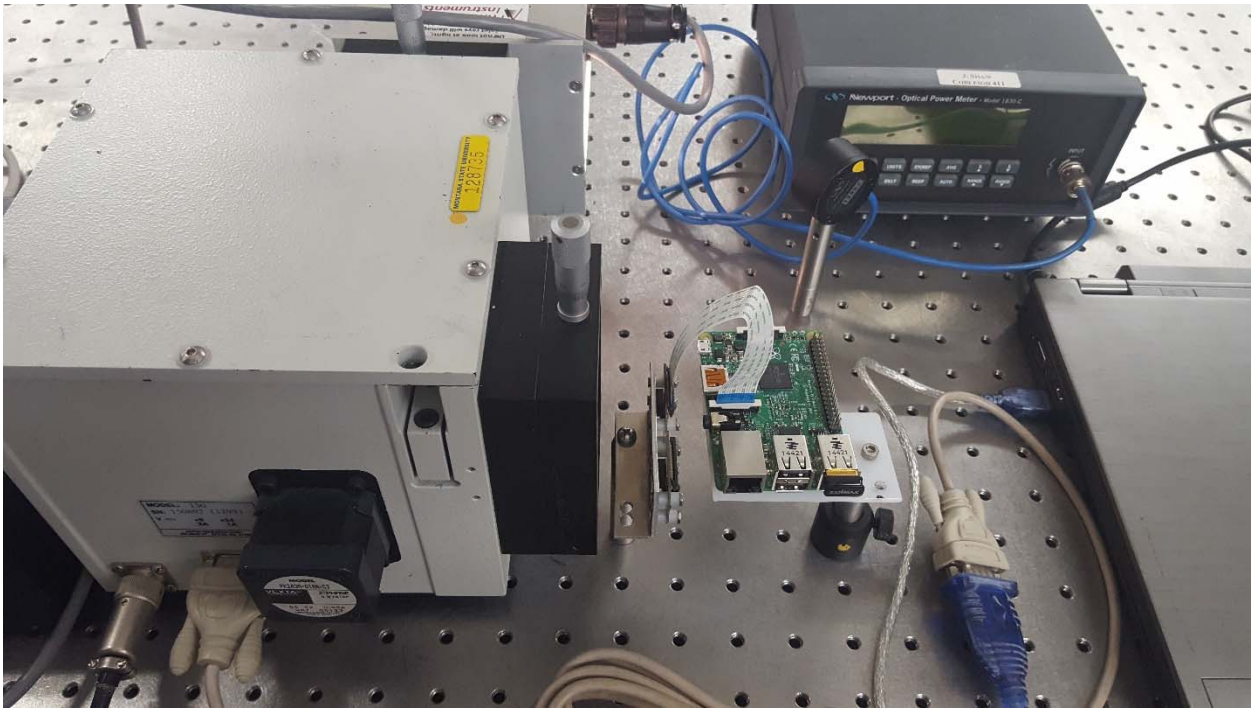

Figure 6. Experimental setup for measuring camera spectral response.

Ultra-compact Thermal IR Camera Calibration

The FLIR Lepton (Fig. 7), an ultra-compact thermal camera, provides a radically smaller thermal imaging capability that could prove useful for imaging in agriculture, forest fire detection and management, and a wide range of urban and ecological studies from UAV platforms. We are using our state-of-the-art capabilities in uncooled thermal camera calibration to determine how well we can calibrate these ultra-compact thermal imagers. We developed software for automated calibration data collection and used a blackbody source and a temperature-controlled chamber to record initial calibration measurements. Data were collected from two temperature sensors on the imaging module, one on the focal plane array (FPA) and the other on the circuitry behind the FPA (auxiliary temperature sensor).

Initial calibration results are encouraging, as indicated in Fig. 8. This figure shows the camera's signal calibrated as radiance [W/(m^2 sr)]. During these measurements the Lepton camera was pointed at a blackbody source whose temperature was increased periodically in a staircase fashion. The yellow line shows the Lepton signal without processing for thermal stabilization. This signal exhibits large fluctuations around the correct value because the camera's response changes with the camera temperature. The red line shows the Lepton signal with our custom thermal stabilization algorithms. During these initial tests we discovered that the performance of the shuttered Lepton is affected by heat generated when the shutter is activated. We are in the process of developing a method to perform a nonuniformity correction to compensate for this thermal effect.

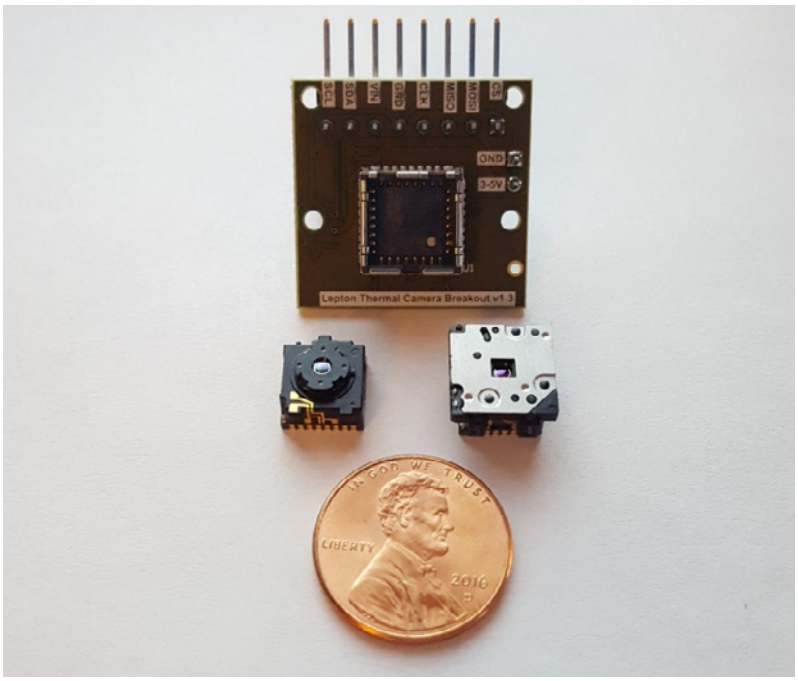

Figure 7. Lepton Thermal Camera Breakout Board, FLIR Non-shuttered and Shuttered Lepton ultra-compact Thermal Cameras.

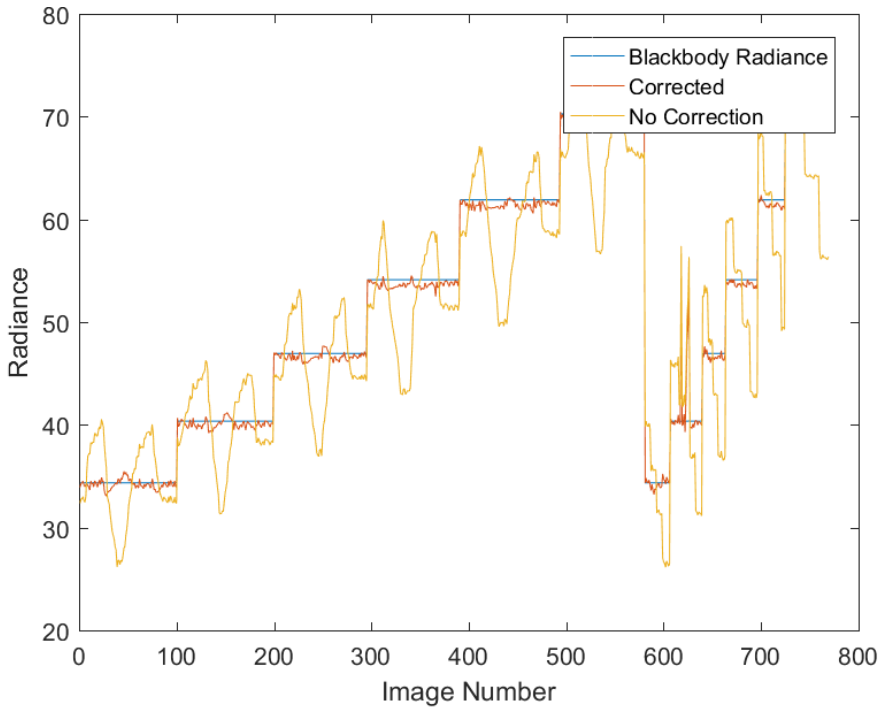

Figure 8. Initial FLIR Lepton Calibration. The blue line is the radiance value for a staircase-stepping calibration source, the yellow line shows the calibrated output of a Lepton imager without our custom thermal-stabilization algorithm applied, and the red line is the calibrated output after the camera's changing response was corrected with the thermal-stabilization algorithm.

Airborne Laser Sensor System

We are developing an airborne laser system to fly in small airplanes for ecological and agricultural studies. The current system is optimized to use a green laser (532-nm wavelength) for lakes, but a future version can combine the green beam with the presently blocked near-infrared beam (1064-nm) for range-resolved vegetation measurements in forestry, ecology, and agriculture. The present system flies on a single-engine aircraft, but we are working toward a smaller system that could fly on a UAV.

The system performed well in test flights this year, but we continue to struggle with the limited data bandwidth provided by the current USB 2.0 data acquisition system. The current system uses a single USB connection for the laser, GPS, imaging camera, time-control server, inertial navigation unit, digital-to-analog detector gain controller, trigger-delay generator, and two channels of high-speed signal digitization. The laser is capable of operating at 120 pulses per second, and if we were to capture 2048 samples for each pulse, this would generate approximately 1 megabyte of data each second. This is too much data to be transferred into the computer rapidly, which limits our acquisition rate to 50 pulses/s.

There are currently no USB 3.0 digitizers of sufficient bit-depth and speed available on the market; therefore, we are discussing with Dr. Ross Snider's group to work toward a solution using his high-speed FPGA-based data acquisition system in development for waterfall sorting and hyperspectral imaging.

Figure 9. Photograph of the MSU airborne lidar installed in the rear of a Cessna 185. The two receiver telescopes and the laser are mounted above a hole in the cabin floor. The electronics, battery, and inverter sit behind the pilot and the lidar operator in the rear of the plane.

Expenditures to date (Grant 41W410) Personnel $92,688.60., Benefits $22,687.64., Operations $24,971.01., Sub Award $64,058.82, total Expenditures **$204,406.09**

Subproject 2: High-performance, real-time image processing for hyperspectral imaging (Ross Snider, rksnider@ece.montana.edu with Resonon, Inc.) Design a high-speed hyperspectral waterfall sorting system to fuse object edge information with hyperspectral data to sort agricultural products quickly and efficiently using Resonon's Hyperspectral Imagers and remove rejected items via air jets. The goal is to perform the data fusion, accept/reject decision, and removal all in real-time using FPGA technology.

Milestones

a) February 1, 2016: Determination of center of mass of each food item in image/line scan
b) September 1, 2016: Determine trajectory of food item for precise timing removal
c) February 1, 2017: Integrate hyperspectral data within food item edge boundaries
d) June 31, 2017: Use hyperspectral data within food item edges to classify food item as accept/reject
e) June 31, 2017: Time air jets to remove rejected food items
f) June 31, 2017: Final report emphasizing commercial products and potential

Progress toward objectives

The air jet subsystem is being put together by undergraduate Sam Kyser. Sam is a dual major in Mechanical Engineering and Computer Engineering, who also has machining skills. He has designed a test bed system that incorporates the manifolds and has assembled the test fixture that will be used to test the air jets. A primary goal is to characterize the air jet latency. Sam is currently building the instrumentation/electronics to characterize the latency. A picture of Sam is shown in Figure 10 with the test system assembled.

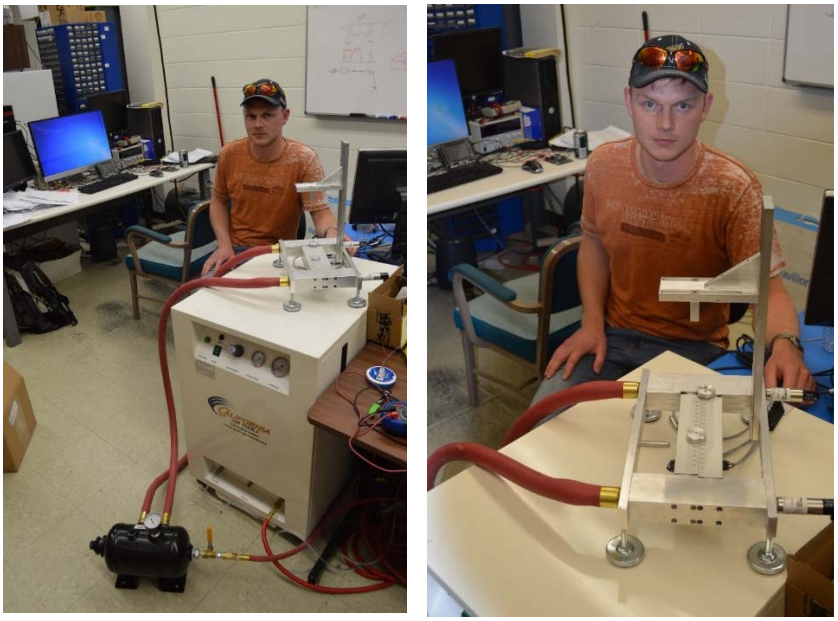

Figure 10. MSU undergraduate student with the air jet subsystem.

We are currently gearing up to test how a simple small hole drilled in the manifold will function as an air jet and we have several diameters of air jets to test. We are sizing the air jets so that we can target lentils as the small grain to sort.

We have purchased a feeder machine (model shown in Fig. 11) that can control feed rates of nuts/seeds/grains from a few pounds per hour to 2 tons per hour. The feeder tray is 4 inches wide and where the product falls off is where we will scan with the hyperspectral and monochrome line scan cameras. The air jets will span the 4 inches of the output of the feeder tray where there will be 32 air jets spaced 1/8 inches apart, which will be suitable for sorting lentils. This is a better solution than conveyor belts that we were originally thinking of using.

Figure 11. Model of feeder for controlling feed rates of nuts/seeds/grains from a few pounds per hour to 2 tons per hour.

The Arria V FPGA board (large square board with blue fan in Fig. 12) is the board that will process the monochrome line scan camera that can generate 640 Mbytes/sec. FPGA daughter cards (on table beneath the camera link cables) have been design to interface the camera to the FPGA board. The camera link FMC-to-FPGA daughter card that is plugged in the board shown in the picture unfortunately does not work with the monochrome camera, so we have to create our own interface. The other FPGA board (rectangular with black fan) is the Arria 10 that will process the hyperspectral data. High-speed serial links (6 Gbps) will send data between the FPGA boards.

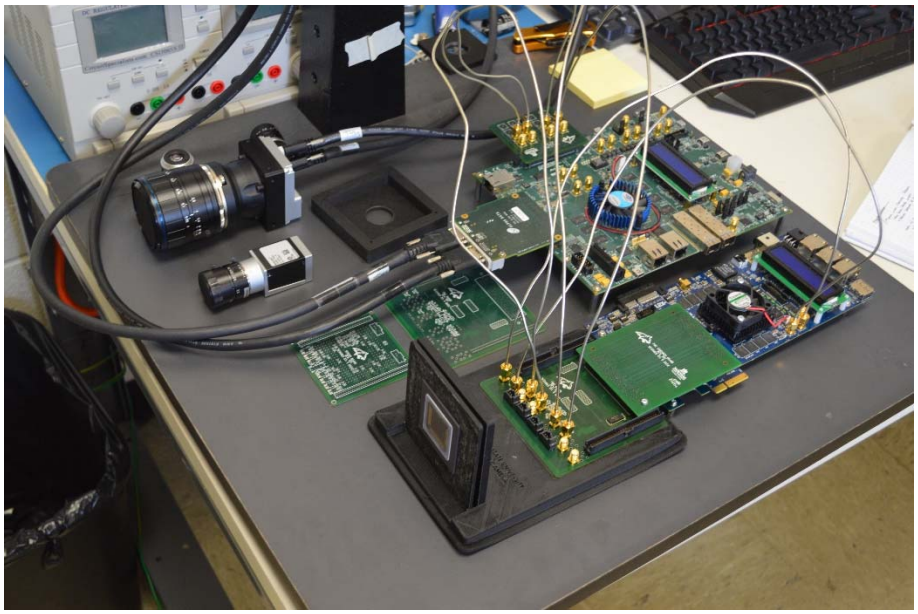

Figure 12. FPGA-based electronics for high-speed hyperspectral image data acquisition.

Projected next quarter activities

- Create air jet manifold that is 4 inches wide with 32 air jets.
- Control air jets via FPGA GPIO.
- Continue with physically integrate line scan camera to Arria V FPGA board.
- Get high speed serial link communication working between FPGA boards.

Expenditures to date (41W411)

Personnel to date $14,107342., Benefits $638.11. Operations $32,648.60., Capital equipment $4845.00, Total Expenditures **$52,239.13**.

Subproject 3: Remote Sensing Algorithms for Precision Agriculture (Rick Lawrence with Resonon, Inc.) Develop and apply a methodology using hyperspectral imagery for determining optimal narrow spectral band combinations for identifying targeted invasive weeds in specific crops.

Milestones

a) July 31, 2016: Collect invasive weed field data
b) August 31, 2016: Collect hyperspectral image data
c) October 31, 2016: Complete image preprocessing
d) January 31, 2017: Complete analysis of spectral band optimization and weed species mapping
e) June 30, 2017: Final report, including applications for commercial site-specific agriculture

Figure 13. Tarp used to locate target signature areas in aerial imagery.

Progress toward Objectives

- Flight plans created and executed for data collection at half-meter resolution without gaps between swaths.
- Two fields flown and ground survey data collected. Due to a programming error, data from one field does not meet project requirements.
- Ground survey data collection of ASD spectral signatures and GPS location of weed and clean (weed-free) areas.
- Data from sensors and field notes processed and moved to central storage system.
- Initial analysis.

Figure 14. ASD spectrometer used to measure on-ground reflectance.

A Resonon Pika II hyperspectral instrument was carried on a Cessna aircraft over one field in Cascade County, MT and two fields in Gallatin County, MT. Weed infested and non-infested areas were identified and marked with tarps, seen in Figure 13, prior to flight to enable positive location on the imagery. Flights were conducted early May and June based on farmer's herbicide spray schedule. Field data were collected on the same day as hyperspectral flights. Missed data during the first flight due to a sensor error resulted in it being unusable for this project. An ASD field Spectroradiometer, shown in figure 14, was used during the June field campaign to collect field-based hyperspectral data as a backup to flight data. Preliminary profiles for wheat and weeds created by compiling ASD data in *R* are shown in Figure 15. Figure 16 shows a processed image of a field from the June flight

campaign in false color IR. Processing included correcting for plane movement and lighting variation during flight. Tarp GPS data were used to stitch data swaths together to create a single image.

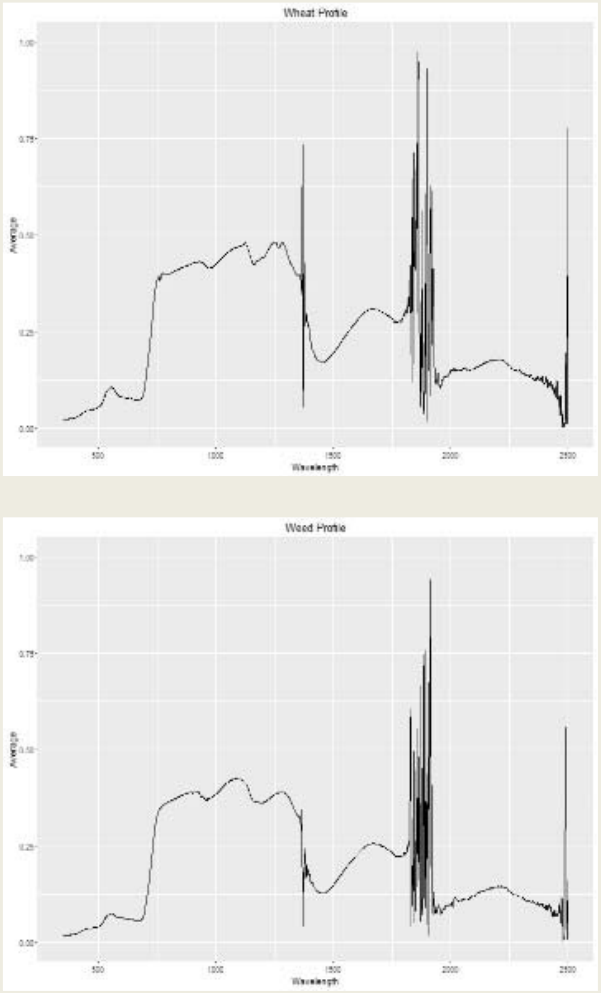

Figure15. ASD Spectral profiles with bands containing values greater than 1 and less than 0 removed.

Figure 16. False IR image of data collected for Western field

<u>Expenditures to date</u> (Grant 41W417) Personnel $23,930.22. Benefits $2,300.98., Operations $4,599.54 total Expenditures **$30,830.74**

Subproject 4: Machine Vision Algorithms for Precision Agriculture (Neda Nategh with Resonon and NWB Sensors, Inc.) Develop machine vision algorithms for weed detection and food sorting using spectral imaging data.

Milestones

a. Sep. 30, 2016 Initial testing of machine vision algorithms complete.
b. May 31, 2017 Final testing and development complete.
c. June 30, 2017 Final report completed.

Progress toward objectives

- Students were advised on the analysis of hyperspectral image data
- Several new proposals were funded based on a similar idea proposed in the MREDI Optics project.
    - "A real-time computational model and algorithm for vision based detection and tracking of orbital debris" – NASA - $50,000.
    - "A biologically inspired algorithm to detect, segment and track moving objects with observer motion" – NSF - $172,000.
- Another new proposal is being prepared for submission in the near future to NASA: "Space debris identification and tracking system based on a real-time, bio-inspired motion processing algorithm," $750,000.

Expenditures to date (Grant 41W413) Personnel $51,186.17., Benefits $3,651.72., Operations $5,286., total Expenditures **$60,123.89.**

Subproject 5: Microcavity sensors for hyperspectral imaging (Zeb Barber with Advanced Microcavity Sensors LLC). Advance MSU/Advanced Microcavity Sensors LLC (AMS) technology on microcavity hyperspectral imaging sensors toward commercial applications in agriculture and engineering tests to determine feasibility of mounting sensor technology on UAV; secondary objective solving MT problems in agriculture and biomedical (skin cancer). The primary objective focused on MREDI goal #2: creating private sector jobs.

Milestones

a) June 1, 2016: Investigate non-circular symmetric micro-cavity mirrors for transverse mode manipulation
b) September 1, 2016: Evaluate Microcavity Hyperspectral Imaging prototype system for early crop disease/weed detection
c) December 30, 2016: Determine engineering specifications for use of Hyperspectral Sensor on UAV
d) June 30, 2017: Submit final report specifying technical accomplishments and outlining commercial potential.

Nontechnical highlights

- Advanced Microcavity Sensors and MSU Spectrum Lab have been informed by the Montana Board of Research and Commercialization Technology (MBRCT) that their proposal, "Light Emitting Diode Pumped Laser Array for Ultra-Spectral Imaging," has been selected for funding in the amount of $129,168. This project extends the microcavity technology to a new promising area.

Technical Progress toward Objectives

a) Advanced Microcavity Sensors and MSU Spectrum Lab have been collaborating on the metrology (measurement) of the laser ablated craters created by AMS. Techniques utilizing optical interferometry have been developed to provide simple accurate measurement of the depth and profile of the craters. This work is being performed currently on MBRCT funding, but will be continued on the MREDI funding this next quarter.
b) As discussed in last quarterly report, the Spectrum Lab came to the conclusion that most agricultural applications are ill-suited to the high spectral resolution provided by the LCAM. For this reason, we have re-evaluated application areas more suited to the LCAM. Two areas standout: passive optical sensing of atmospheric gases and the microcavity-based dye laser application that will be funded by the MBRCT. The passive optical sensing of atmospheric gases application is interesting because it takes advantage of the high spectral resolution of the LCAM technology. Absorption lines of trace gases in the atmosphere can have very narrow resonance widths on the order of 10 GHz (0.02 nm in the NIR) (see Figure 17) or even less, which is higher resolution than most spectrometer technologies but within the limits of the LCAM. This quarter we plan on using the MREDI funds to produce LCAM units in the NIR to test against the atmospheric oxygen lines.

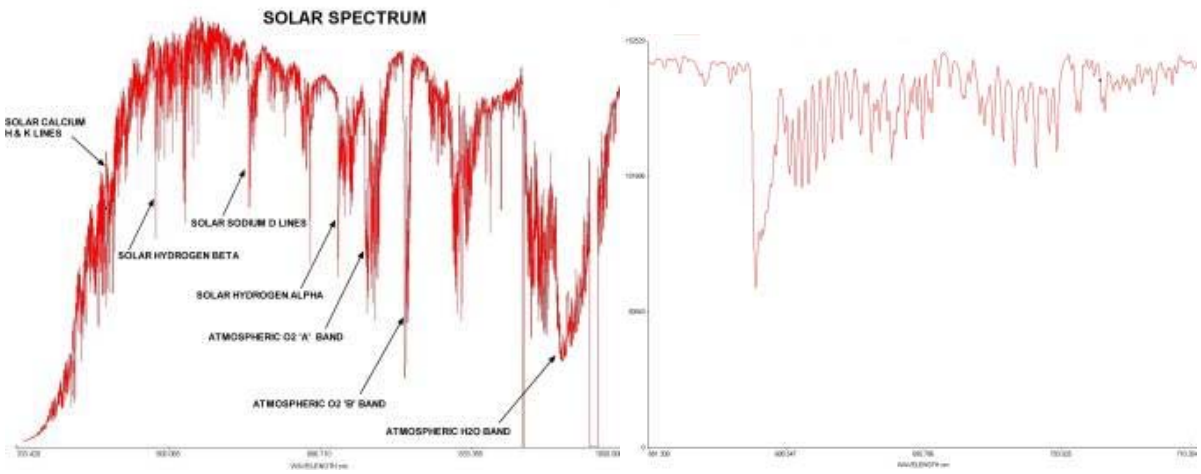

Figure 17. (Left) Solar spectrum and (right) zoom of the atmospheric oxygen "A" band from Optomechanics Research, Inc. webpage. http://www.echellespectrographs.com/gallery.htm#ao2.

In anticipation of applying for additional funding for the microcavity-based dye laser application, MSU Spectrum Lab has performed some initial work on the MREDI funding. In this work we put together a microcavity cell that is filled with Rhodamine 6G dye dissolved in ethylene glycol. We then illuminated one of the microcavities with 520 nm laser illumination and observed enhanced dye fluorescence in the cavity region (See Figure 18). This experiment clearly showed enhancement only when the laser was coupled to the microcavity; however, clear laser-like threshold performance has not been observed as yet. Work in this area will be continued on the MREDI and MBRCT funding.

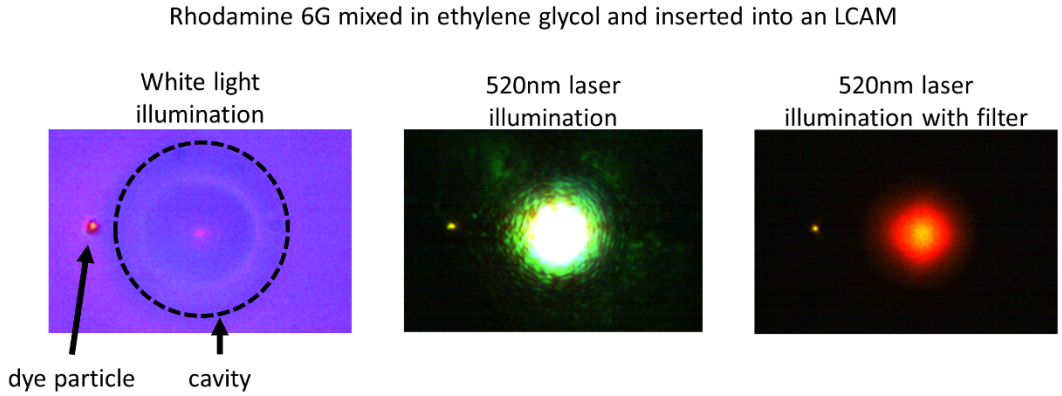

Figure 18. Initial results of a dye-based LCAM laser. Rhodamine 6G is a very common dye used in lasers that can be pumped in the blue-green part of the spectrum to lase in the orange-red part of the spectrum.

c) No progress to report this quarter.

d) No progress to report this quarter.

Expenditures to date (Grant 41W418) Personnel $9834.64 Benefits $3446.08 Operation $460.29., total Expenditures **$13,741.01**

Subproject 6: Hyperspectral imaging for monitoring cell growth (Ed Dratz, dratz@chemistry.montana.edu with Resonon, Inc.). Design a hyperspectral imaging system for monitoring the metabolic state of live cells in culture. Applications to stem cells for understanding disease mechanisms in individuals, drug testing in cells from individuals, potentially optimize personal nutrition, and solve Montanan's health problems.

Milestones

a) February 1, 2016: Complete design and testing of proof-of-principle prototype hyperspectral imager with improved cost/benefit, prototype interface for cell hyperspectral analysis, and development of stem cell labeling.
b) May 1, 2016: Integrate the prototype systems for advanced analysis of stem cell metabolism with hardware and software control. Test for evaluation of optimization of selected nutrients.
c) October 1, 2016: Refine and improve software and operating conditions of real time hardware and software for variations of metabolic state for culture optimization.
d) February 1, 2017: Enhance user interface to control system and software to control and optimize nutrient composition; evaluate possible changes in microscope system for improved performance.
e) June 30, 2017: Proof of principle for feedback control of nutrient optimization with nutrient dosing control system. Investigate biochemical individuality in pilot experiment.
f) June 30, 2017: Submit grant proposals to leverage additional support. Final report to MUS that summarizes accomplishments and commercial potential.

Activities to date

The inverted epifluorescence microscope optical system has been designed, optical vendors contacted for providing optical modules, the optical system has been configured, and all the microscope components ordered, as reported in the Q3 report. As we explained in Q3, we were able to find a single vendor, ASI, to provide an integrated, high-performance inverted microscope solution, where all the components are sure to fit together with appropriate focal lengths and where the specialized hyperspectral components can be fitted. Furthermore, we note in this Q4 report that this US vendor will provide the best possible price on the complete optical systems. This excellent price for the optical components will facilitate the commercialization of the complete hyperspectral microscope with the integrated microfluidic cell culture system and complete, powerful computer control and software system that is under development.

We have an upright, laser-excited fluorescence microscope test bed at Resonon for testing the hyperspectral microscope system. We expect that the hyperspectral components in hand can be integrated with the modular inverted microscope, as soon as the inverted microscope parts arrive. The inverted microscope system is essential for viewing live cells and monitoring their metabolic state, which is at the center of this project. We are working to resolve a problem that has arisen with the procurement of the optical components for the integrated inverted microscope system. We are again revising the procurement paperwork and expect the essential optical components to be ordered soon.

A particularly critical component is the computer-controlled XY sample stage, which has to be able to scan in small, very high resolution steps for maximum hyperspectral resolution (22 nm in this case), along with rapid movement speed (7mm/sec in this case), so we can rapidly revisit cells in the field for repeated spectral measurements after modifying the nutritional state. The same microscope vendor (the only U.S.-based microscope manufacturer) got its start as a successful company by designing, building and selling high-performance digital microscope stages, which another reason we are convinced that this vendor is the most suitable for our application. The ASI Company has also expressed interest in teaming with us to refine the development of our planned commercial product.

The microscope will do an initial rapid scan of the image field, the software will locate cells, and the cells will then be scanned at high resolution repeatedly during the course of the experiments. Thus, the stage has to be able to scan rapidly between cells and then switch to much slower, small step sizes for high-resolution imaging. The software control for the XY stage and Z automatic focusing with programmable nose piece for changing objectives for different magnifications has been designed. The upright epifluorescence microscope test system from the Dratz Lab that was moved to the new Resonon facility is being used for initial testing of the excitation laser system for hyperspectral imaging.

The Onix CellAsic microfluidic cell culture control and observation system for controlling and optimizing the nutrient media has been installed on the refurbished laser- confocal, with the latest image analysis software, that is important for providing benchmarks for the new hyperspectral system. The Zeiss LSM 510 meta is a high performance confocal, with the latest image analysis software, that is important for providing benchmarks for the new hyperspectral system. A second, improved version of the Onix CellAsic microfluidic system has been released since we purchased the initial system and Millipore is providing us with the latest model at no additional charge, as a partnership, as they believe that our hyperspectral system will generate many customers for their CellAsic microfluidic system. Prof. Snider's team is working on the software to integrate the Onix CellAsic microfluidic culture control with the hyperspectral data acquisition and processing.

A great deal of progress has been made in the Dratz lab on introducing optogenetic probes of the oxidation/reduction state into human adult stem cells in culture. The probes have been transferred to efficient carrier vectors that are providing improved, more facile optical probe introduction.

We have also introduced the optogenetic probes in to Murine smooth muscle cells to demonstrate the wide applicability of our systems for metabolic monitoring of live cells (Figs. 19, 20). There is a great deal of local experience with these smooth muscle cells and monitoring the control of the metabolic state if these cell lines. A graduate student in the Dratz lab is devoting full effort to working with the optogenetic probes, assisted by a research undergraduate, two postdoctorals in the Reijo Pera lab, and Robert Usselman, a Reseach Assistant Professor in the Singel lab, all in the MSU Chemistry and Biochemistry Department. An advanced undergraduate Electrical and Computer Engineering (ECE) Design Team in the Snider lab in ECE is continuing to design the microscope stage controller system and the controller for the cell culture environmental control system. A graduate student in the Snider lab is devoting full effort to the high-speed hyperspectral imaging analysis software and will be working on

this crucial aspect of this project into the next year. The personnel include two graduate students devoting full effort to the project, two advanced undergraduates on an ECE Design team.

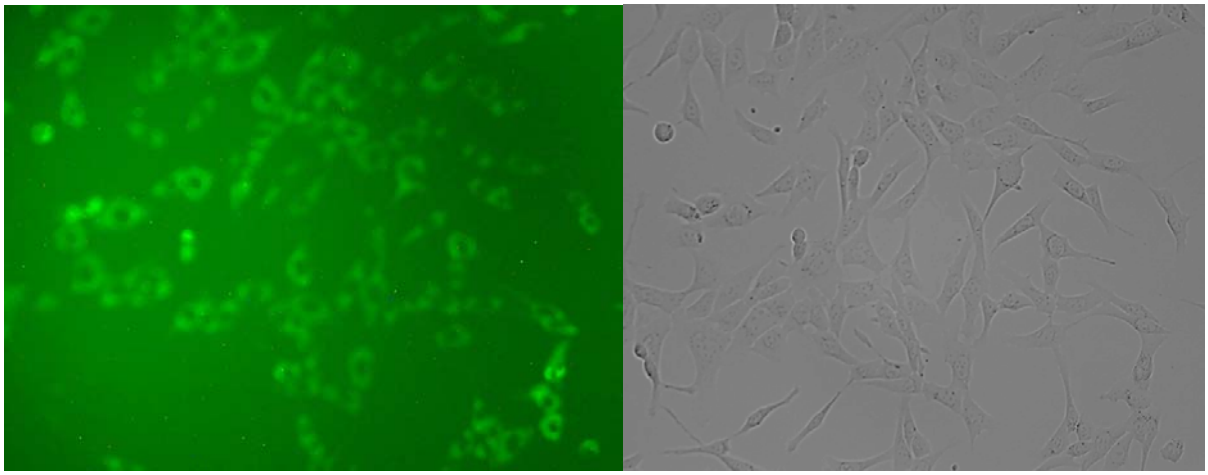

The open areas in the cells correspond to the nuclei, since the probes are targeted to mitochondria, but single mitochondria are not resolved at this 10x magnification.

Bright field image of same region of the cell culture as shown in the fluorescence image on the left.

Figure 19. Murine smooth muscle cells transfected with Mitochondrial-targeted roGFP2 (GSH/GSSG sensor).

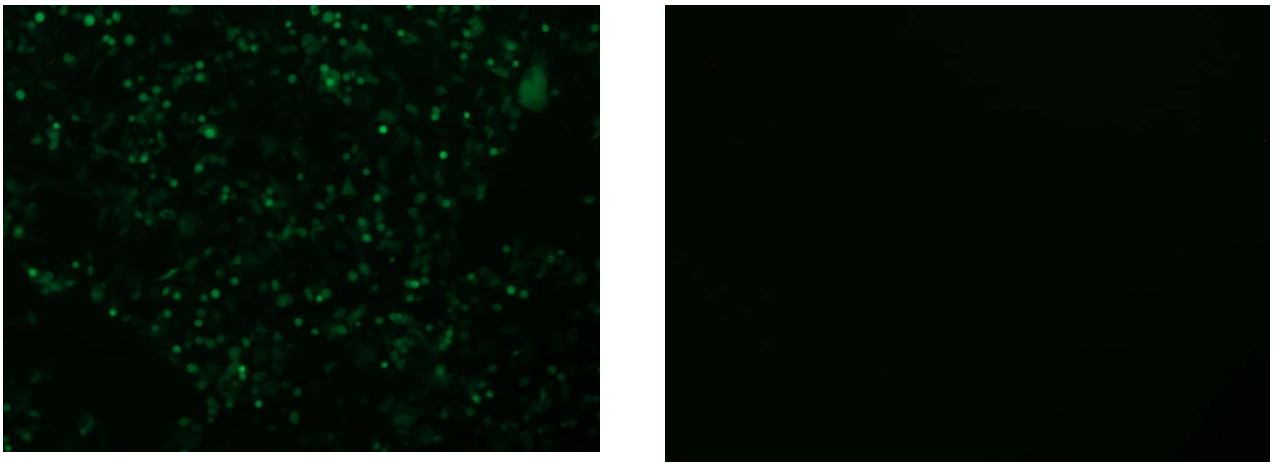

Figure 20. hiPSCs + Mito roGFP-ORP1, targeted to mitochondria: (left) Plus H202 oxidation and (right) Minus H202.

Expenditures to date (Grant 41W414) Personnel $35,127.89 Benefits $2551.74 Operations $18,621.74, Capital Equipment $29261.20 total Expenditures **$85,562.57**

Subproject 7: Translational research to commercialize micro-mirror technology (Arrasmith at Revibro Optics). Translate MSU-developed deformable mirror technology to a commercially sustainable product.

Milestones

a) June 30, 2016: Refine production to achieve a repeatable fabrication process. This milestone will involve a redesign of fabrication masks, purchase of new wafer bonding equipment, and refinement of wafer bonding process
b) Obtain funding from another source. Revibro will pursue funding through commercial sales and commercial R&D efforts (June 2016), and through SBIR/STTR or similar government funding (June 2017)
c) Create 2 full time Montana jobs: One job will be created immediately to sustain the founder of Revibro – August 2015; Technical and/or sales and marketing hire – December 2015

Progress toward objectives

- Published a conference proceedings paper and recently had a journal paper accepted documenting temporal performance of Revibro's deformable mirrors
    - In collaboration with Chris Zhang, a PhD student under Dr. Dickensheets
- Had attended the Hannover Messe trade show in Germany as part of the Montana Pavilion – this is the largest industrial automation trade show in the world, with over 120,000 attendees
- Pursuing other funding opportunities
    - Submitted a Nine Sigma proposal for an extended depth-of-focus microscope
    - Submitted a Phase I SBIR proposal
- Completed a new mask design for improved fabrication of deformable mirrors

During Q4 Revibro Optics supported efforts by Chris Zhang, a PhD student at MSU, to publish the results of the high-speed performance characterization done during Q3. This resulted in a conference proceedings paper entitled *Dynamic performance of MEMS deformable mirrors for use in an active/adaptive two-photon microscope*, published through SPIE. Revibro has continued to work with Chris Zhang to publish these results in a peer reviewed journal article. The paper has been recommended for publication, and Revibro is currently supporting Chris with recommended revisions to the paper. This paper will be the first peer reviewed Journal associated with Revibro Optics, and will provide credibility and exposure for our novel technology.

Revibro Optics attended the Hannover Messe trade show in Hannover, Germany the last week of April (Fig. 21). As part of a Montana-sponsored pavilion, Revibro joined several other Montana companies in this opportunity to get some international traffic to our technology. We received several good leads both from people passing by our booth, and by walking around the venue with fliers in hand to target specific potential customers and early adopters. This Montana-sponsored pavilion was a great benefit for international exposure. While in Germany, we were also able to spend two days meeting with a key early customer, and had the opportunity to see our prototypes in use within their test systems and new product designs. Continued interaction with this customer will likely result in an OEM supply agreement

for Revibro Optics in the next two years. Keeping this relationship active was an invaluable part of the trip to Germany.

Figure 21: Revibro Optics shared booth space with other Montana small businesses at the Hannover Messe trade show in Germany (MREDI funds were not used for the international travel).

Pursuing other funding sources continues to be a high priority for Revibro Optics. In addition to pursuing commercial sales and gaining exposure through shows like Hannover Messe, Revibro submitted two proposals during Q4. We will continue to pursue funding opportunities through both private

organizations like Nine Sigma and government programs like the SBIR program. Hopefully we will hear the results of these first two proposals during the next quarter.

Working toward Milestone A, Revibro completed a new fabrication mask layout for improved MEMS devices during Q4. We will be fabricating and testing these improved devices during Q5. During Q3 we found that the cost of commercial wafer bonding equipment that would greatly benefit our fabrication is prohibitively expensive, so we plan design and build a wafer bonding device in-house. This bonder will improve upon the current apparatus that has been used for several years, and hopefully provide better device yield and performance. The design of this new bonding device will be synergistic with the fabrication of improved mirrors in the next two quarters.

Revibro continues to search for an appropriate new hire. We are looking for an entry-level engineer, or technical sales person to complement our team. Hiring another full time position will be a great step for Revibro, bringing our full time employees to two people and fulfilling Milestone C of this project.

Total Expenditures: (Grant 41W410 Sub-Award) Personnel & Benefits $64,058.82, total Expenditures **$64,058.82.**

Subproject 8: Active waveguides and integrated optical circuits (Rufus Cone, cone@physics.montana.edu, collaborating with Babbitt, Nakagawa, Barber, Himmer, Avci, and Thiel with S2 Corp., AdvR, FLIR/Scientific Materials, and Montana Instruments). Integrate Montana products, expertise, and capabilities to improve marketability, performance, and enable additional products: Build interdisciplinary connections among MUS and Montana optics industries to integrate (a) optical crystals by FLIR/Scientific Materials Corp. (SMC); (b) waveguide photonic components of AdvR, Inc.; (c) Montana Instruments (MI) cryogenic systems; and (d) S2 Corp. (S2C) signal processing devices.

Milestones:

a) Fall 2015: Fabrication of rare earth doped optical waveguide suitable for optical signal processing applications
b) Summer 2016: Integration of an optical waveguide into a cryostat
c) Spring 2017: Demonstration of SSH processing in a cryogenic waveguide
d) June 2017: Final report summarizing technical results and emphasizing commercial potential

Activities to date

During this fourth reporting period, significant progress continued on all project activities and our second major milestone was successfully achieved. Coupling of laser light to both planar waveguides and AdvR's single-mode channel waveguides at cryogenic temperatures of only 3K above absolute zero was demonstrated in the Montana Instruments cryostation. Using several methods and exploiting the unique sample access and configurability of the Montana Instruments product, we were able to obtain total optical efficiencies of up to ~10%, a surprisingly high value considering the losses in our initial arrangements. Coupling to a rare-earth-activated planar waveguide in a Tm:YAG spectral hole burning S2 signal processing crystal at 3K was also demonstrated, as shown in Fig. 22 – a significant step towards achieving our next project milestone.

Figure 22. Coupling of laser light into and out of a rare-earth-activated waveguide at 3K within a Montana Instruments C2 Cryostation.

A wide range of coordinated research and development activities are progressing rapidly at this stage of our effort, most of which are in close daily collaboration with our Montana industrial partners. In particular, MSU personnel are working with AdvR Inc. to transfer their waveguide lithography and fabrication techniques to the MSU research program, while also developing at MSU new characterization techniques that will be transferred to AdvR to enable enhanced product performance. MSU students have developed and fabricated new crystal mounts for the Montana Instruments cryostat and are investigating advances in thermal shielding and sample control in the cryogenic environment. At the same time, a series of new rare-earth-activated $LiNbO_3$ optoelectronic crystals have been grown by Scientific Materials Corp / FLIR and are being characterized at MSU for waveguide applications; new ideas are being developed to expand Scientific Materials Corp's capabilities to produce new types of crystal products. All of this work has been coordinated with new activities at S2 Corp and in direct support of their recent multi-million-dollar contract (as described in the previous report and press releases),

with additional contracts expected in the near term. In particular, new insights gained on this MREDI effort into microscopic material physics as well as sources of environmental noise disturbance of the signal processing crystals are are leading to improved performance and better modeling of design requirements such as thermal loads and mechanical isolation.

Several MSU students working on this project received degrees during this quarter, and all of those students are already employed working on research and development related to their MREDI research experiences at MSU. Brett Wilkins received his B.S. degree in physics and is working for AdvR Inc. in the production and characterization of their waveguide products.

In addition to those selected highlights from this quarter, additional outcomes are outlined below.

Progress on Technical/Educational Objectives:

- *Coupling light into optical waveguides at cryogenic temperatures:* A number of methods for coupling light into a waveguide held inside a cryostat have been investigated, with help from AdvR, Inc.. Approaches considered and tested included focusing with combinations of micro-ball lenses, GRIN (gradient index) lenses, precision achromatic lenses, direct fiber coupling, and microscope objectives. The simplest and most efficient approach that we have tested so far couples into the waveguide with high-quality achromatic lenses located outside the cryostat, and images the back face of the waveguide with a small lens inside the cryostat. Coupling into both planar and channel waveguides at low temperature in the Montana Instruments Cryostation has been successfully achieved. Efficiencies on the order of 10-15% are observed, with further improvement expected as coupling techniques and designs improve. We have applied these techniques to demonstrate coupling to both rare-earth-activated planar waveguides in the cryostat and single-mode channel waveguides fabricated by AdvR Inc., as shown in Figs. 23 and 24, respectively.

Figure 23. (left) Direct optical fiber coupling to a Tm:YAG planar waveguide. (center) Output laser beam and diffraction fringes from the planar waveguide. (right) Coupling light into and out of the Tm:YAG planar waveguide at 3K in the Montana Instruments Cryostation.

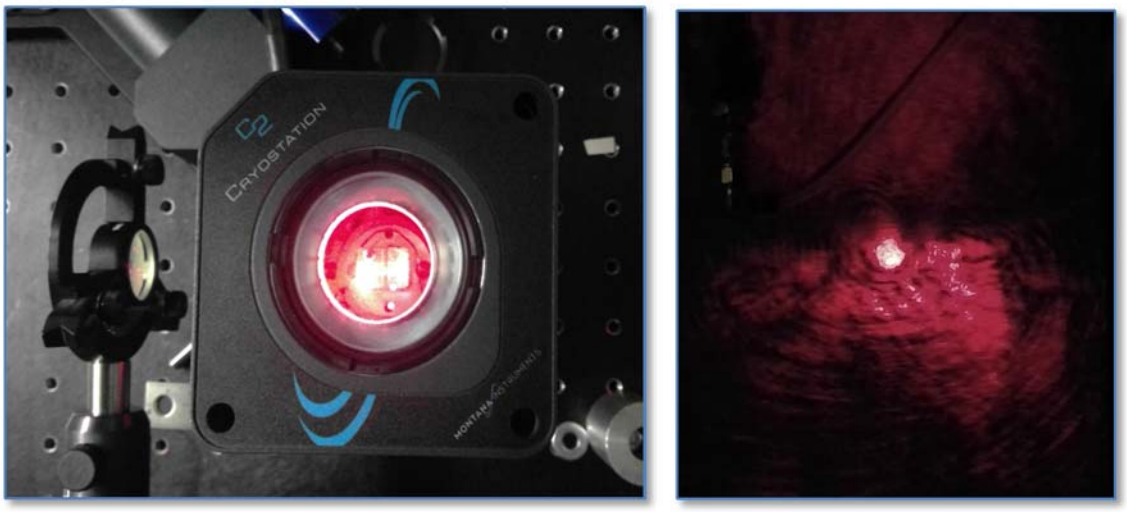

Figure 24. (left) Coupling light into and out of an AdvR Inc single mode channel waveguide held at 3K in the Montana Instruments Cryostation. (right) Output laser spot from the AdvR waveguide.

- *Optical lithography and waveguide fabrication in lithium niobate crystal wafers:* Toward the objective of constructing optically active waveguide circuits, Spectrum Lab Research Engineer Tia Sharpe continued detailed training in microfabrication, lithography, and optical waveguide process techniques. The general photonic waveguide fabrication steps include the following: a) design and fabricate a lithography mask, b) deposit layer of SiO_2 over wafer, c) spin coat photoresist onto wafer, d) expose resist based on mask patterns, e) develop and remove exposed resist, f) etch SiO_2 from resist free areas, g) remove remaining resist, h) perform proton or ion exchange, i) dice wafer, and finally j) test efficiencies.

  Personnel on this MREDI effort are working closely with Bozeman optics company AdvR while learning photonic waveguide processes. AdvR's Briana Jones (Fig. 25) illustrated the company's poling process that is used to create light wave frequency doubling waveguides. Sarah Mondl of AdvR (Fig. 25), a regular MSU MMF customer, has been training Tia Sharpe on waveguide fabrication processes in lithium niobate (Fig. 26). A mask that was specifically designed, fabricated, and used for some the processes detailed in this section is depicted in Fig. 27. Tia worked with Tim Fry of AdvR to learn their mask drawing procedures then ordered masks from Photo Sciences. These test systems will be used to determine general loss characteristics of waveguides, a topic of interest to AdvR. Four new wafers are now waiting in queue for the proton exchange process and subsequent dicing. AdvR, and MSU's SL and Cone labs will have access to the new waveguides for characterization once these processes are completed.

Figure 25. AdvR professionals working on waveguide fabrication processes with MSU personnel. (left) Briana Jones of AdvR prepares poled waveguide wafer for HF etch bath under AdvR's vented fume hood. (right) Sarah Mondl of AdvR positions a LN wafer in MSU's MMF Cobleigh Hall cleanroom within the Angstrom sputter system in preparation for SiO_2 deposition.

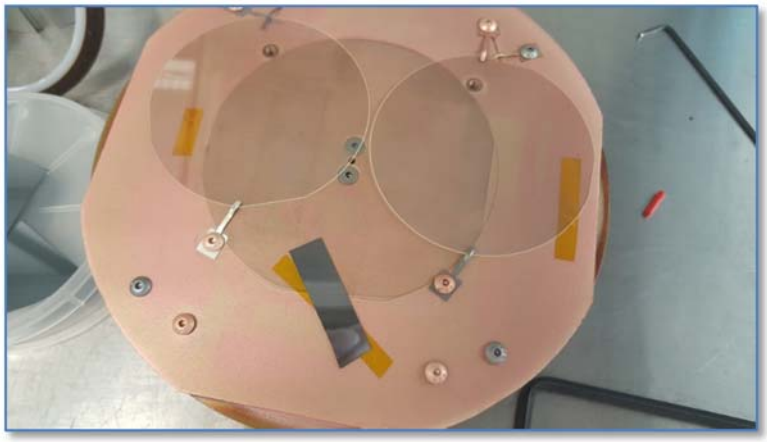

Figure 26. Two LN wafers and a small piece of Si "witness" wafer mounted on the Angstrom sputter system deposition plate.

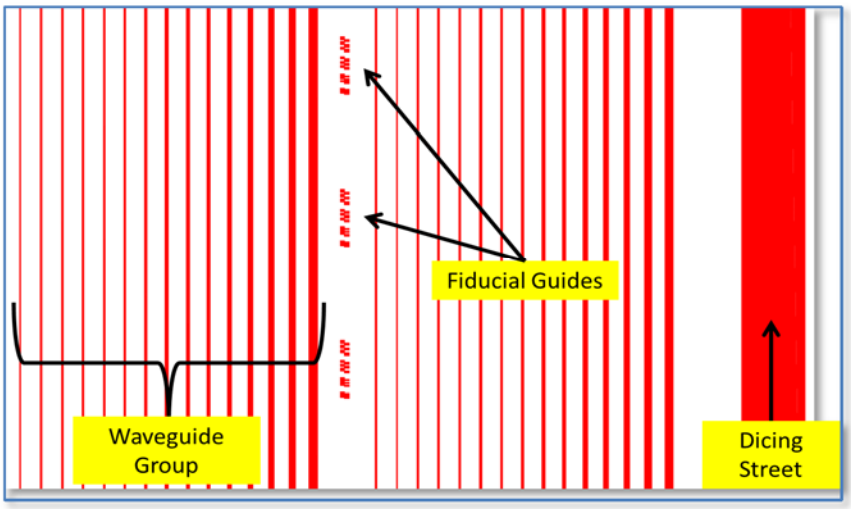

Figure 27. Lithography Mask Pattern. Linear waveguide design has all channels the length of the mask, two groups of 15 channels separated by 150 µm and channels separated by 50 µm. The two groups of channels are separated by 500µm including a dicing street. The pattern is repeated many times over the width of the mask. Channel widths are 2, 2.5, 3, 3.5, 4, 4.5, 5, 6, 7, 8, 10, 12, 14, 16, and 20 µm wide. Fiducial widths are 2, 3, 4, and 5 µm wide, 10 µm long.

- *Testing lithography photoresist quality:* Results of testing lithography using old S1813 photoresist compared to newer AZ-1512 photoresist are shown in Fig. 28, demonstrating that there are large differences in how evenly the photoresists may be spin coated onto wafers. The photo in Fig. 28(a) shows some irregularities on a photonic wafer after photo resist development during the initial phase of this project. The irregularities shown on and close to the waveguides (light green lines) cause excess power loss and reduce propagation efficiencies. The photo in Fig. 28(b) illustrates a much improved result after new photoresist and development.

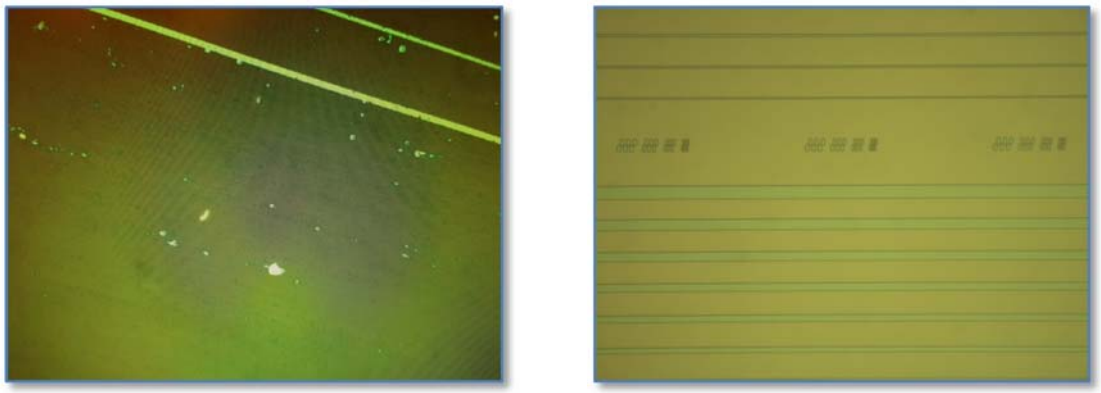

Figure 28. (a) Poor photo resist coverage showing inconsistencies on photonic wafer section after photoresist development. Clumps in photoresist cause reduced yield and power losses in straight waveguides (light green lines). Application techniques needed improvement and new photo resist was used in (b). Smooth photo resist coverage of photonic wafer section seen in (b) after photo resist development. The smooth waveguides are ideal for low loss light propagation. The small features toward the top of the figure are fiducials; periodic 2, 3, 4, and 5 µm wide features with 50% duty cycles that give a measure of merit to the photo resist exposure and development times.

Anytime new photoresist is used, the lithography mercury lamp exposer energies and solvent development times are tested to ensure the best features. The photos in Fig. 29 were taken after the photoresist was developed. The effects of overexposure can clearly be seen at the higher exposure levels.

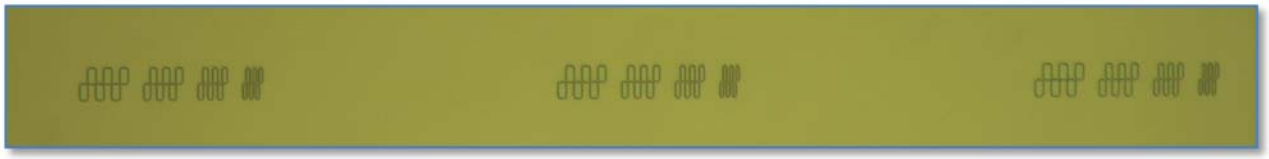

(a) 35 mJ (area 1)

(b) 105 mJ (area 8)

Figure 29. Fiducials of test wafer with exposure energies as noted to explore the effects of overexposure of photoresist on the lithography process. In (a) the features are clear and symmetric although the rectangles are a little rounded indicating a slight over development time. In (b) the features are smeared because of over exposure. All photos taken with camera coupled microscope with x20 magnification.

- *Lithium Niobate Crystal Growth at MSU:* Very small $LiNbO_3$ samples have been successfully grown from melt at MSU using the equipment and supplies acquired during our MREDI work, providing an important step toward the new capability to supplement and support the large-scale crystal growth efforts at Scientific Materials Corp. Parameters of the growth are actively being refined. Future crystal growth designs and plans involve dipping an air-cooled ceramic rod tipped with a seed crystal into the melt, with adjustments to temperature stabilization as necessary.

- *Diffusion doping of rare earth ions into $LiNbO_3$:* Both Tm^{3+} and Er^{3+} rare earth ions have been successfully indiffused into LiNbO3 crystal wafers by depositing thin metal films on the surface of wafers in a deposition chamber at high vacuum, then treating them at high temperature for up to 100 hours. The indiffusion depth profiles have been characterized by ToF-SIMS in ICAL. Precise depth calibration is actively in progress by using ICAL's AFM, as is waveguide characterization at AdvR with M-Line Spectroscopy. Sources of contamination have been eliminated and manufacture process parameters have been well-determined through scientific literature review and analysis of experimental results, directly expanding the MSU capabilities in material development as well as opening new possibilities for optically-active waveguides to be developed for industrial uses. Use of higher-quality metal vapor deposition instruments at MMF is in progress as a route to refine material and waveguide development for transition from the lab to industry applications.

- *Waveguide Wafer Endface Polishing Process Development at MSU:* The Cone Group has been able to successfully polish endfaces of waveguides of various types to allow direct optical coupling. The waveguide is placed in an adjustable aluminum chassis, then covered completely in mounting wax for mechanical stability. Increasingly fine grades of polishing pads are then used to remove defects on

the endfaces. The quality of the finish and therefore the light coupling efficiency is expected to improve with more refined technique, materials, and tools.

- *Fabrication of proton exchanged waveguides in rare-earth-activated crystals at MSU:* Undergraduate researcher Kyle Olson, with the help of graduate students Aaron Marsh and Tino Woodburn as well as AdvR, successfully fabricated proton-exchanged $LiNbO_3$ planar waveguides at MSU. The exchange modified the extraordinary refractive index making a guiding layer that is 3-4 microns deep with several supported guiding modes. Material composition was determined with ToF-SIMS at MSU ICAL. The guiding characteristics were determined with M-Line spectroscopy at AdvR, Inc. Plans to improve the quality of wafer cuts by use of AdvR's dicing saw are in progress. Further work includes indiffusion of different rare earth ions to investigate the effect of proton exchange on the optical fluorescence, spectral bandwidth, and fundamental waveguide properties.

- *Testing Vibrationally Induced Coherence Loss in Closed-cycle Cryostats:* In this quarter, we completed initial investigations of the vibrationally induced coherence loss in two locally produced low vibration closed-cycle cryostats. Optimal performance of spectral holographic processing devices, in waveguides and bulk, depends on achieving the long coherence times afforded by spectral spatial (S2) materials. The S2 material coherence times can be degraded due to the stresses or vibrations introduced during the cryocycling of a closed-cycle cryostat. The physics behind this loss in coherence is still an open question. Developing techniques for measuring these coherence losses and their time dependence will help in the investigation of the physics of this phenomenon as well as in the design of practical cryostats for S2 processing devices.

  Montana Instruments and S2 Corporation, both located in Bozeman, are the world leaders in the development of low-vibration closed-cycle cryostats. The first cryostat we tested was the Cryostation C2 produced by Montana Instruments (MI). The second cryostat was a Cryomech PT405 cryocooler with a modified sample chamber and mount built by S2 Corporation (S2C) and acquired by MSU several years ago. In both cryostats, the same Tm:YLuAG (3% Tm in a 50% Yttrium, 50% Lutetium crystal) crystal was directly mounted to each cryostat's vibrationally isolated sample mount, with varnish used for the MI system and cryogenic grease and copper tape used for the Cryomech/S2C system. The MI system employs a Gifford-McMahon refrigeration cycle. The Cryomech system tested employs a pulse tube refrigeration cycle. Both cryostats were operated at their lowest temperature, both achieving 2.8K, as indicated on their system temperature sensors.

  MSU Physics graduate student Aislinn Daniels (pictured in top of Fig. 30) built the current setup (illustrated in bottom of Fig. 30) to measure the coherence times and coherence losses during the cryocycle with the earlier help of undergraduate Ryan Galloway and graduate student Torrey McLaughlin. Two types of measurements were made, both relying on timing the experiment synchronized with the cryostat's cryocycle. The MI Cryostation has an output that signals the start of its cryocycle, making synchronization easy. The timing jitter of the MI system was on the order of milliseconds. The Cryomech cryostat did not include an easy electronic means of synchronizing the experiment with its cryocycle. A trigger circuit based on the sensing, filtering, and squaring the sound of the helium gas flow was designed and built. The resultant timing jitter of our measurement of the Cryomech's cryocycle was on the order of 20 milliseconds.

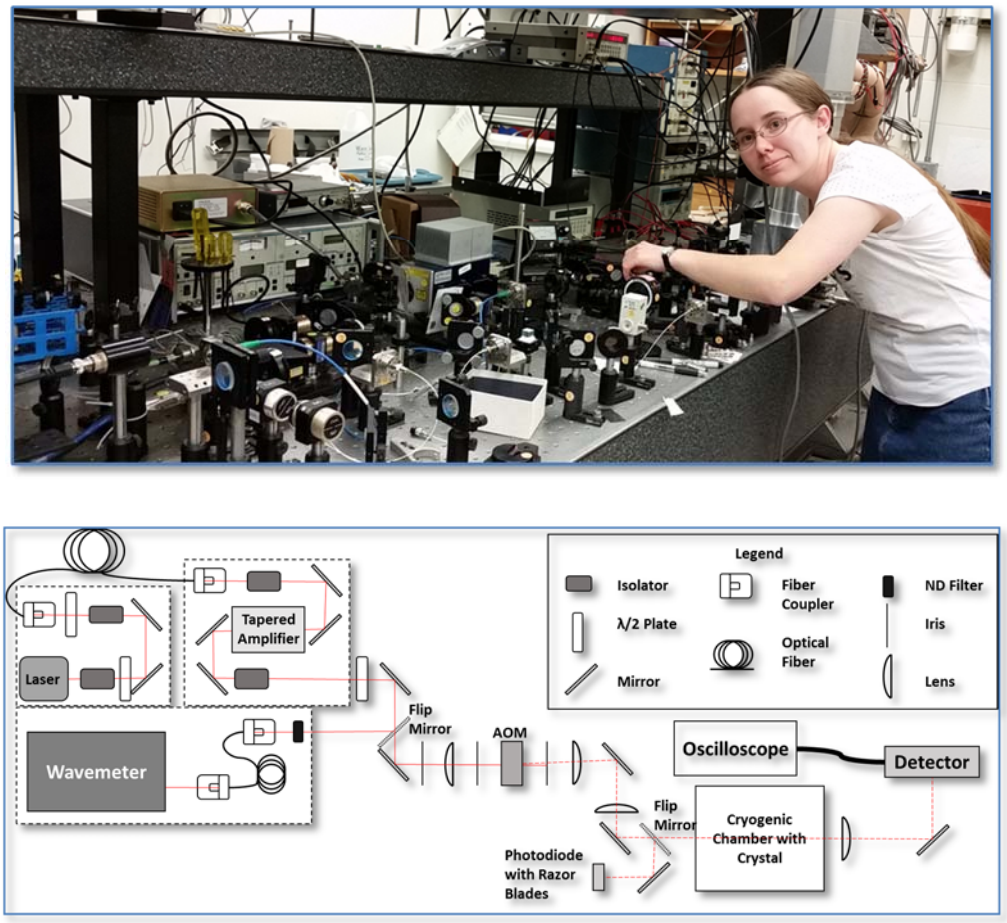

Figure 30. Graduate student Aislinn Daniels (top) and the experimental set-up (bottom) used to make measurements of the vibrationally induced broadening during the cryocycles of closed cycle cryostats.

The first set of measurements employed a two-pulse photon echo technique, with a fixed delay between the input pulses, τ_{21}. The photon echo energy was measured as a function of the experiments delay within the cryocycle, t_{cryo}. The effective broadening due to vibrations, $\Delta(t_{cryo}, \tau_{21})$, at a given delay of τ_{21} is shown in Fig. 31 throughout the cryocycles of the MI Cryostation (left) and Cryomech/S2C cryostat (right). Both cryocycles have a period roughly 710 milliseconds. The vibrations, and thus the broadening, peak twice during the cryocycle, as the valves for helium input and exhaust are opened. The results indicate that the MI system has a measured peak broadening of roughly 5-10 KHz, over twice that of the Cryomech/S2C system (2.5 KHz), while the Cryomech/S2C system has periods of broadening roughly twice as wide as the MI system. Both these levels of broadening are quite narrow compared to closed cycle cryostats without vibration reduction. The differences between the cryostats may be due to systemic errors, such as the jitter in the Cryomech/S2C measurement of t_{cryo}. The difference in mounting (varnish versus grease) could also affect the results, as the varnish mounting (hard at room temperature) may introduce more stress on the crystal as it cools down. Both systems had average broadenings that ranged from 800 to 1200 Hz over their data sets. The conclusion is that both systems were about equal in their vibration reduction within the systematic errors of the testing. The results set a baseline for future measurements.

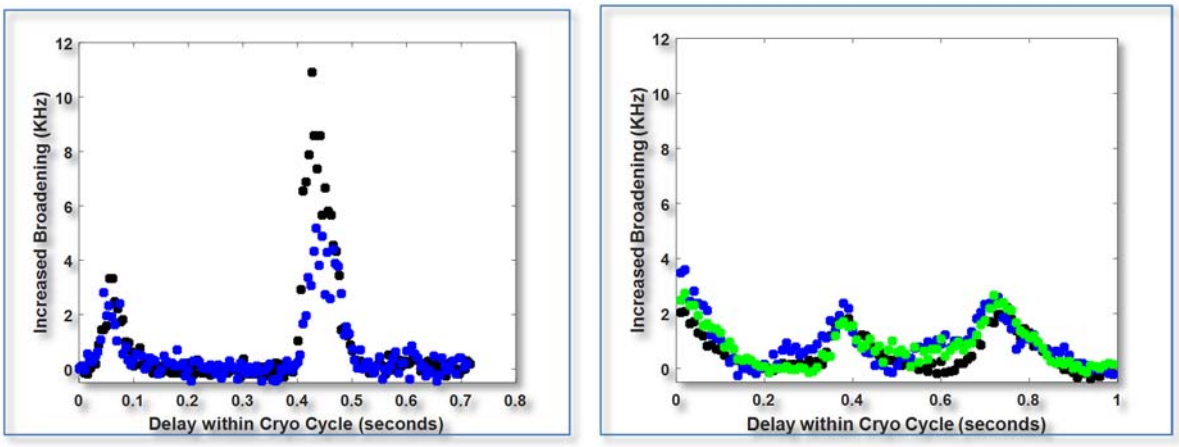

Figure 31. The estimated effective increase in broadening (at τ_{21}=12 microseconds) throughout the cryocycles of the MI Cryostation (left) and Cryomech/S2C cryostat (right).

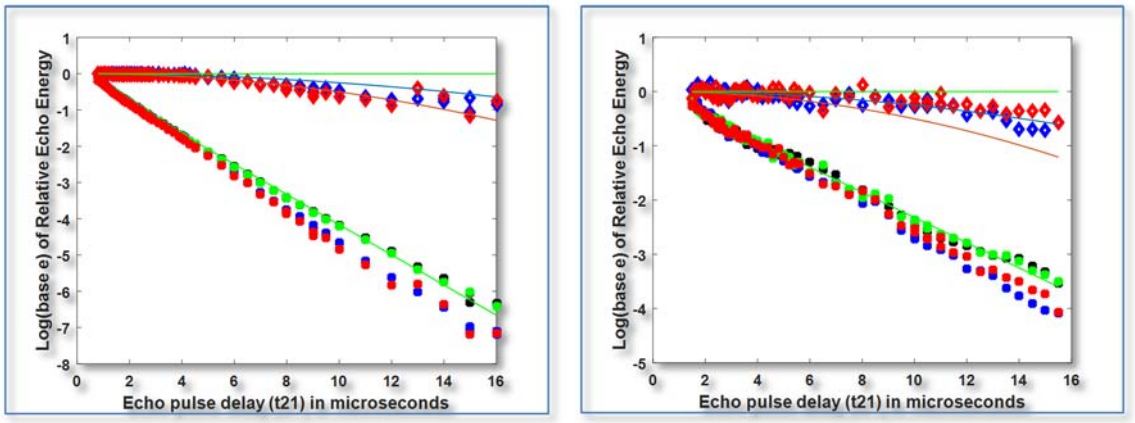

Figure 32. The logarithms of the normalized photon echo energies as a function of τ_{21}, measured at two cryocycle delays, one at a delay with minimal vibrational broadening (green and black points) and one at a delay with peak vibrational broadening (lower red and blue points). The green and black lines are linear fits to the green and black points. The upper red and blue points are the differences between the lower sets of points for the two cryocycle delays for two repeats of the experiment. The blue and brown lines are quadratic curves corresponding to broadenings of 0.2 KHz/microsecond (blue) and 0.4 KHz/microsecond (brown). The MI data is on the left and the Cryomech/S2C data is on the right.

The second set of measurements also employed the two pulse photon echo technique, now with a fixed cryocycle delay, t_{cryo}. The photon echo energy was measured as a function of delay between the input pulses, τ_{21}. Figure 32 (lower four sets of points in each graph) shows the logarithms of the normalized echo energies as a function of τ_{21} for two values of t_{cryo} for each cryocycle. One of the t_{cryo} was when the broadening was negligible and the other was when the broadening was peaked. The experiment was repeated to demonstrate repeatability, thus there are four sets of points per graph. The curves for the t_{cryo} with negligible broadening were fit to a line to determine the T_2 values for each cryostat, which were determined to be 10 microseconds for the MI system and 17

microseconds for the Cryomech/S2C systems. The difference in the T_2 values for the two cryostats indicate a likely difference in the crystal temperatures. This could be due to the crystal in the MI system not being wrapped with copper tape, leading to less cooling of the crystal and a higher shorter T_2. This difference in temperature may also lead to a difference in the broadening. This could be corrected and explored in future experiments.

The upper two sets of points in each graph of Fig. 32 shows the difference of the logarithms of the normalized echo energies as a function of τ_{21}. These data points for the two cryostats were compared to quadratic functions in τ_{21} (blue and brown curves in each graph), with $4\pi\tau_{21}\Delta(t_{cryo}) = 4\pi(0.2\text{kHz/usec})(\tau_{21})^2$ fitting better for the Cryomech/S2C system and $4\pi\tau_{21}\Delta(t_{cryo}) = 4\pi(0.4\text{kHz/usec})(\tau_{21})^2$ fitting better for the MI system. Again the differences in the broadening coefficients may be the result of systematic errors in the measurements and mounting of the crystal.

- *Computer software for analysis of rare-earth-ion wavefunctions in crystals:* Extensive computer programs from Argonne National Laboratory were obtained from Dr. Guokui Liu, an MSU alumnus (Ph.D. with Professor Cone) for describing and refining the optical properties and energy levels of rare earth doped materials for waveguides and other applications, as well as enabling new data analysis for scientific publications. This software can be applied for all of the twelve optically-active rare earth ions that are relevant for our materials and devices.

- *Student Training:* Undergraduate Kyle Olson and Graduate Students Tino Woodburn and Aaron Marsh attended the Montana Photonics Industry Alliance (MPIA) Hamamatsu Training conference. Many different types of detectors, their properties, and their applications to spectroscopy were discussed and lectures on their theory and specifications were given as a part of continuing the attendee's educations as well as developing in-lab skills directly applicable to MREDI objectives. Graduate Students Tino Woodburn and Aaron Marsh also attended an NSF-supported National Nanotechnology Coordinated Infrastructure (NNCI) Montana Nanotechnology Facility (MONT) conference. The conference showcased MSU's measurement and characterization capabilities in many different fields directly applicable to MREDI, but also the attendees were able to give direct input on how to improve inter-lab and inter-departmental collaboration and capabilities through MONT.

- *Theoretical analysis of the effects of spectral hole burning on optical waveguides:* Causality dictates a relationship between a material's absorption spectrum and the index of refraction, a fact that leads to the relationship known as the Kramer's-Kronig relation. This basic relationship suggests that whenever we modify the absorption spectrum of a material, such as to store information with spectral hole burning as done by S2 Corp and MSU Spectrum Lab, that there must also be a corresponding modification of how light refracts or guides through the material. This effect is of fundamental interest since it could be possible that the guiding properties of rare-earth-activated optical waveguides could be either improved or degraded by this mechanism. Consequently, during this quarter graduate student Jacob Braunberger explored the theory of this relationship for the conditions relevant to spectral hole burning applications.
  From this analysis, we find that the maximum possible change in index of refraction Δn due to a change in optical absorption $\Delta\alpha$, such as caused by a programmed spectral structure, is given by

$$\Delta n_{max} = \frac{\lambda_0}{8\pi}\Delta\alpha \qquad (1)$$

From this relationship and using values for the physical parameters characteristic of materials and laboratory conditions, (0.01% Tm^{3+}:$LiNbO_3$ excited near $\lambda_0 = 794$ nm with $\Delta\alpha$ of ~2 cm^{-1}), we find that $\Delta n_{max} = 6 \cdot 10^{-6}$, which is negligible relative to the step index change of at least 0.01 that is typically used to form waveguides. Consequently, our theoretical analysis indicates that the waveguiding properties of these optical devices should not be detrimentally affected by the rare-earth ions in the crystal or by the spectral hole burning process itself, a key positive finding for our effort.

- *Material and waveguide chemical composition characterization at MSU physics and ICAL:* Extensive new optical material property determination has been developed and continues to develop in collaboration with other MSU labs and local optics companies as part of our MREDI effort. ICAL directly provides a wide range of material and surface characterization techniques that are now being regularly employed for this work, including Atomic Force Microscopy, Electron Backscatter Diffraction, and Time of Flight Secondary Ion Mass Spectrometry (with examples of ToF-SIMS and AFM analysis shown in Fig. 33).

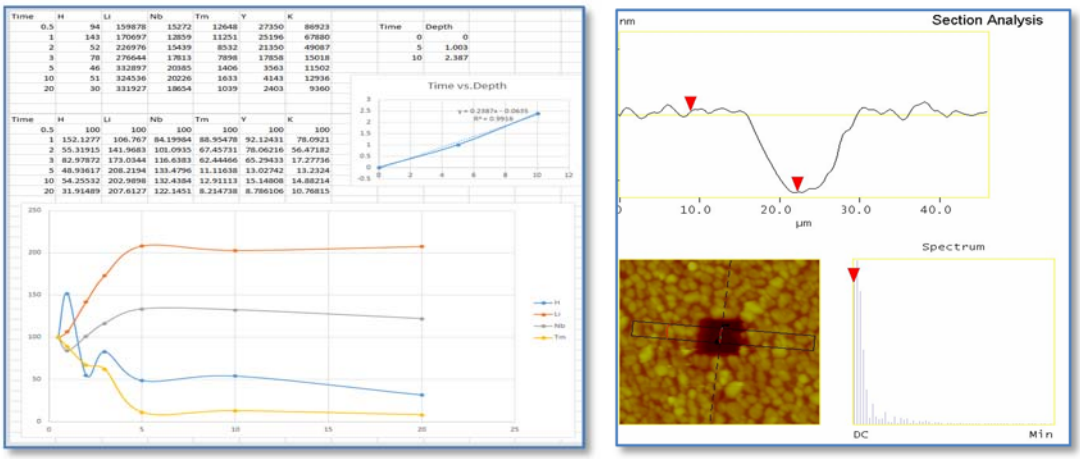

Figure 33. (left) Example ToF-SIMS analysis acquired by students at MSU ICAL showing the chemical composition of a thulium indiffused lithium niobate sample fabricated at MSU as a function of depth below the surface a, showing a Tm diffusion depth of 1 micron, near our target value of several microns. (right) AFM depth measurement at ICAL for the ToF-SIMS sputtering hole profile in the lithium niobate crystal, allowing precise calibration of ion diffusion depths.

Due to the insulating nature of crystalline materials like $LiNbO_3$, many of these measurements are difficult to execute directly, as charge builds up on the wafers as a part of the measurement process and prevents further probing. Dr. Recep Avci and ICAL deposited gold onto the surface of the materials, making it possible for the excess charge to be dissipated. ICAL's measurement capabilities were directly expanded by applying this technique on a $LiNbO_3$ sample borrowed from the Cone Group on their new Nano-Auger. Consequently, the collaboration between the Cone Group and ICAL gives MSU a unique advantage in characterizing insulating materials. Furthermore, the AFM was then used to calibrate the sputtering rate of the gallium ion gun for both the x-cut and z-cut $LiNbO_3$ crystal orientations. The different crystal axes differ in sputtering rates as well as diffusion rates which can be utilized to match desired material and waveguide parameters.

- *Sub-micron poling of ferroelectrics for advanced optical waveguide devices:* Several steps have been made towards the goal of sub-micron periodically poled ferroelectrics for advanced optical parametric

wavelength conversion in waveguides. The long term goal of this work is the development and modeling of sub-micron poling of waveguide devices, which can then be extended to operation into a cryogenic environment. The sub-micron poling capability adds a broader range of operating wavelengths for AdvR's (a Montana optics company) product line, while enabling the conversion to wavelengths compatible with spatial-spectral holographic processing material and are capably of operation in cryogenic environments and integration with spatial-spectral holographic waveguide processing devices. This work is done in collaboration with Prof. Wataru Nakagawa, Professor of Electrical and Computer Engineering and Dr. Phil Himmer, Manager of the Montana Microfabrication Facilities (MMF), and undergraduate student Carol Baumbauer. Nakagawa and Himmer are PIs on a Montana Space Grant Consortium (MSGC) grant on sub-micron poling development. The project is aided by the support of Dr. Philip Battle of AdvR.

Following a comprehensive survey of possible poling techniques, a plan for poling a patterned electrode was developed. The plan required the training of graduate student Torrey McLoughlin (funded 50% by MREDI and 50% funded by MSGC) on many of MSU's MMF's capabilities (see Fig. 34), including the Amod evaporator for the deposition of conducting layers, the spin coater and contact aligner for lithographically patterning electrodes, and acid etching to create the detailed electrode structure. Characterization of our poling success will also be necessary in the future. In order to accomplish this, the graduate student was also trained on the atomic force microscope (AFM) and field emission scanning electron microscope (FESEM) in MSU's Imaging and Chemical Analysis Laboratory (ICAL).

We discussed with AdvR on their poling attempts and the poling voltage source. AdvR agreed to assist the project by allowing access to the voltage source and companion waveform generator. An initial test of characterization capabilities was carried out utilizing lithium niobate and KTP (potassium titanyl phosphate) crystals provided to us by AdvR. Both FESEM and AFM measurements were found to be sufficient for poled KTP however, another method will be necessary for future measurements of poled lithium niobate. Preliminary discussions regarding setting up a piezo-response force microscopy (PFM) were carried out with MSU ICAL staff, and it was decided that these measurements will be practical in ICAL, only requiring a rearrangement of the present AFM setup to characterize poled lithium niobate. To further characterize our poling, discussions with the High-Temperature Materials Laboratory at MSU regarding their wedge-polishing capabilities were carried out to begin a collaboration.

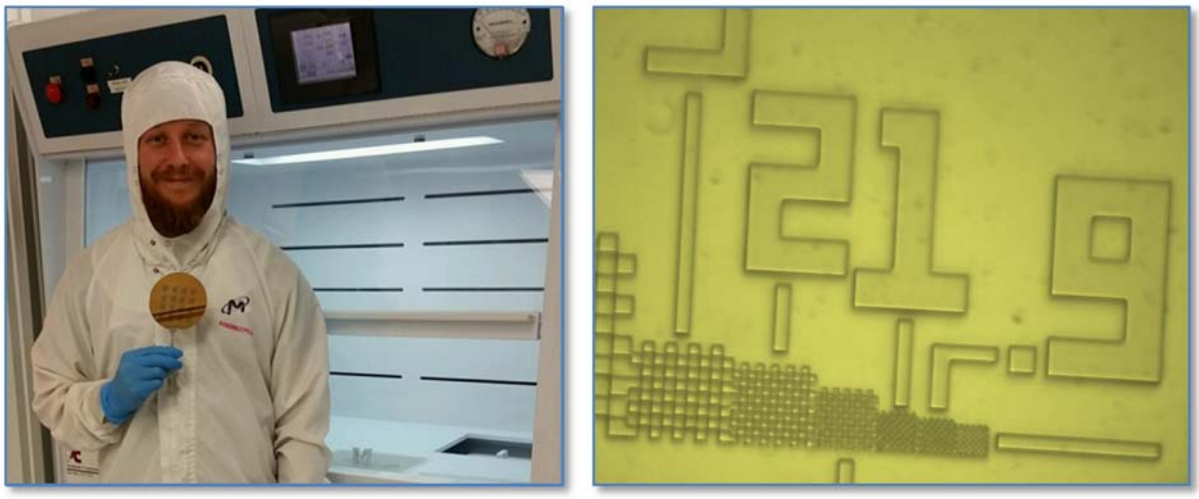

Figure 34. Graduate student Torrey McLoughlin (left) in MSU's Microfabrication Lab, holding chrome on silicon wafer that was coated with gold and photoresist and then exposed and developed to reveal 3, 2, 1.5, 1, and 0.9 micron features (right). The optimal exposure time was determined to be 1.4 second.

A program for designing photomasks was learned and implemented. The photomask designed was ordered and received from University of California Santa Barbara's California NanoSystems Institute. The photomask contains many electrode patterns that will be lithographically created and tested as poling sources. In line with the goals of generating sub-micron poling, many of the electrodes were reserved for patterning with electron beam lithography in MSU ICAL; that will allow nanometer scale features.

A process to lithographically pattern the gold electrodes was created, and testing of several steps in the process has taken place. Silicon and fused silica wafers were coated with a thin chrome layer (to help with adhesion) followed by a thicker layer of gold. The thickness of the metal layers was measured to gauge the accuracy of the system's deposition rate and to perfect the layer's thickness on future depositions. The wafers were spin coated with photoresist in preparation for photolithography. A study of UV exposure times was carried out in order to maximize the lithographic feature resolution by avoiding under or over-exposing the photoresist. Now that the exposure times for gold on chrome silicon are optimized, the next step is to optimize etch rates for both the gold and chrome; those tests are currently ongoing. In next quarter fabrication of gold electrodes and demonstration of poling of KTP using the techniques developed for sub-micron poling will be carried out.

- *Design of new lithography masks for testing rare-earth-activated waveguide devices:* Working with AdvR Inc personnel, MSU research engineer Tia Sharpe designed and acquired custom optical lithography masks for producing test waveguide structures in rare-earth-activated crystals. In addition to incorporating different sizes of channel waveguides to optimize coupling and transmission, optical splitters and interferometer elements were incorporated to provide initial testing platforms for advanced waveguide signal processing architectures. Some of these basic mask designs for these waveguide device components are illustrated in Fig. 35.

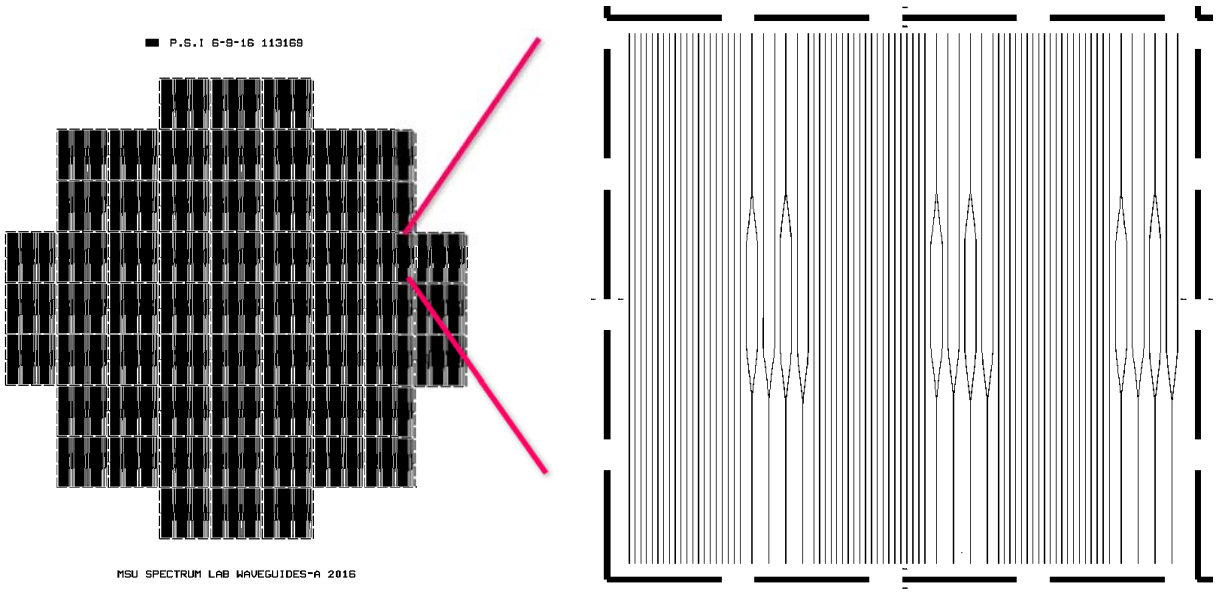

Figure 35. Example of 3" diameter lithography mask designed and obtained by MSU Spectrum Lab for fabricating optical waveguides with different sizes and basic photonic structures, such as optical splitters and interferometers.

- *Optical waveguide theoretical modeling and computer simulations:* New waveguide model development using the COMSOL Multiphysics software continued during this quarter. Models for description of wave propagation in guiding structures similar to those being developed in our crystals are in progress. Discussions are underway with local companies on joint projects enabled by this new capability at MSU. Examples of waveguide modeling results for more advanced designs such as buried waveguides with better optical coupling efficiency are shown in Fig. 36.

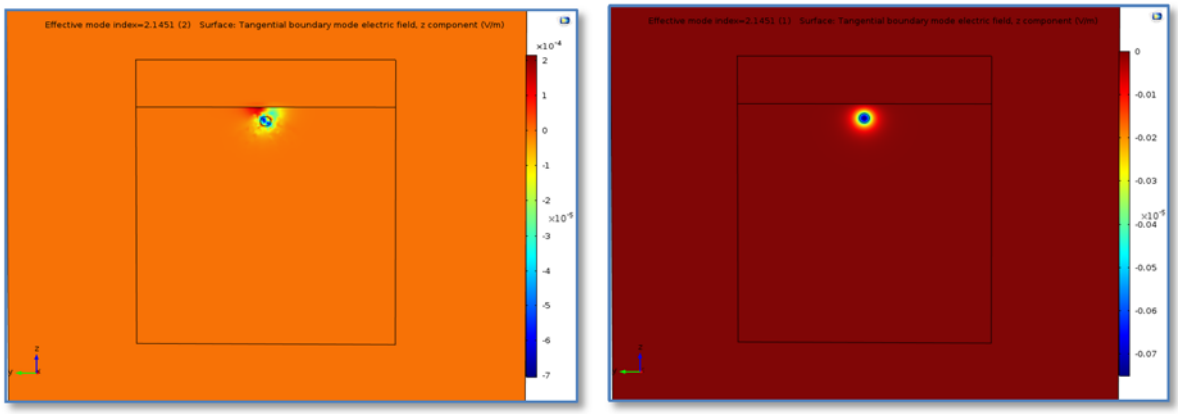

Figure 36. (left) Example COMSOL modeling of an optically lossy mode in an alpha phase reverse proton exchanged $LiNbO_3$ buried channel waveguide, indicating that there may be enough of an interaction between the surface and the guide for light to leak out of a buried channel guide that is very close to the surface (3 microns from center of guide to glass edge in this instance), illustrating a typical aspect of waveguide design that may be explored with this software. (right) Ideal mode simulation of a shallow buried channel waveguide.

- *Investigation of Li^+ out-diffusion effects in $LiNbO_3$:* Lithium out-diffusion in $LiNbO_3$ is currently being investigated, both as a waveguide fabrication technique and also as a means to increase the permeability of $LiNbO_3$ to produce waveguides with deeper rare earth and proton exchange layers. COMSOL Multiphysics simulations (see Fig. 36) and discussions with Dr. Zeb Barber of Spectrum Lab suggest that there are significant interactions between the surface and the waveguide that contribute to scatter and loss. By "burying" the waveguides deeper within the crystal wafer, scattering loss from surface effects and interactions will be minimized, producing a more robust, higher-quality waveguide that can be developed with small changes to current manufacturing processes. For this approach, the material processing, optimization, and characterization remain in progress.

Progress on Economic Objectives:

Figure 37. Brett Wilkins completed his MSU Physics B.S. degree and is now employed at AdvR Inc. helping develop their optical waveguide products.

- During this quarter, undergraduate student Brett Wilkins, shown in Fig. 37, completed his Bachelor's degree in Physics at MSU while working on this MREDI effort. After graduating from MSU, as a direct result of this MREDI effort Brett applied for a job at AdvR. Inc. in Bozeman, MT and was subsequently hired for a position to help with producing and characterizing their waveguide products.

- During this quarter, undergraduate student Kaitlin Poole completed her Bachelor's degree in Physics at MSU while working on this MREDI effort. After graduating from MSU, received a commission as an active duty second lieutenant assigned to the Information Directorate of the Air Force Research Lab (AFRL) in Rome, NY, where her title is Physicist. Kaitlin achieved her immediate career goals as a result of this MREDI work and her Air Force ROTC training, and she plans to continue with her professional career in lasers and photonics development. Kaitlin and her family were residents of Bozeman, where her father works in health care.

- Graduate student Aaron Marsh was awarded a Master's degree en route to a Ph.D. in Physics while working on this MREDI effort.

Figure 38. Undergraduate Kyle Olson wrote a successful USP summer research proposal to study the effects of waveguide fabrication on rare-earth-ion optical properties.

- While working on this MREDI effort, undergraduate student Kyle Olson (sophomore in Physics), shown in Fig. 38, wrote and submitted a successful summer research proposal that was funded by the MSU Undergraduate Scholars Program. Kyle's summer project is directly related to our MREDI goals and involves studying the effects of waveguide fabrication on the properties of rare-earth ions in crystals. During this quarter Kyle has been working in the Cone research lab, regularly interacting with AdvR Inc. to develop waveguide fabrication techniques and working with MSU ICAL to characterize the atomic composition and spatial profiles of the waveguides that he creates and studies.

- During this quarter, visiting Fullbright Postdoctoral Scholar Dr. Rose Ahlefeldt, who assisted with work on this MREDI effort, completed her one year stay at MSU and returned to Australia to continue work on rare-earth-activated materials for quantum information applications. Collaboration continues on

research and development between MSU and the Australian National University research group she is joining.

- Prof. Thomas Böttger from the University of San Francisco visited MSU from June 22 to July 1 to contribute to research efforts on this MREDI effort. All of Prof. Böttger's travel and living expenses for this effort were paid for by the University of San Francisco.

- Dr. Charles Thiel and Rufus Cone were invited to present results from this MREDI project at the California Institute of Technology on May 25-26, 2016 by Professor Andrei Faraon of the Applied Physics Department. They also met individually with many members of the Department. Our collaboration with Professor Faraon's research group has already produced a publication accepted to appear in Physical Review B **94**, 045134 (2016), entitled "Optical spectroscopy an decoherence studies of Yb^{3+}:YAG at 968 nm." Professor Faraon is sending two senior researchers to our MSU lab for experiments during August and September 2016, and Faraon has accepted our invitation to visit our MSU lab and research group and to present a Physics Colloquium lecture at MSU on October 7, 2016.

- Dr. Charles Thiel (Senior Research Scientist, MSU Spectrum Lab and Physics) gave an invited plenary lecture at the 19th International Conference on Defects in Insulating Materials (ICDIM'16) in Lyon, France on July 11, 2016. The topic of this lecture was materials research at MSU related to our MREDI effort as well as highlighting the capabilities and significance of the extensive Montana optics and photonics industry. This presentation was recorded by the conference organizers and will be posted on the internet for broader dissemination. All travel expenses to give this presentation were paid for by the conference organizers and the National Science Foundation.

- Dr. Zeb Barber presented recent collaborative work with S2 Corporation on high bandwidth real-time matched filtering at the IEEE Summer Topical Meeting on Photonic and Analog Hardware Accelerators for Energy Efficient Computing July 11-13th in Newport Beach, CA.

- Dr. Zeb Barber gave presentations at the Conference on Lasers and Electro-Optics (CLEO) June 7th, 2016 in San Jose, CA. He presented recent collaborative work with S2 Corporation on high bandwidth real-time matched filtering.

- Dr. Charles Thiel presented work related to our MREDI efforts for the 19th International Conference on Dynamical Processes in Excited States of Solids (DPC'16), at Chimie ParisTech, Paris, France on July 21, 2016. The topic of this talk was to explain the unique capabilities of spectral hole burning laser frequency reference technologies patented by MSU and licensed to the Montana company S2 Corp.. All travel expenses to give this presentation were paid for by the National Science Foundation.

- Dr. Charles Thiel presented work related to our MREDI efforts for the Chimie ParisTech 2016 Rare earth workshop in Paris, France on July 25, 2016. The topic of this talk was materials research at MSU related to our MREDI effort as well as highlighting the capabilities and significance of the extensive Montana optics and photonics industry. In particular, the role of Montana companies in international research and development efforts was discussed. All travel expenses to give this presentation were paid for by the National Science Foundation.

- Professor Rufus Cone finished a one academic year term as Deputy Director of the MSU Optical Technology Center (OpTeC).

- Professor Rufus Cone and Dr. Charles Thiel received an MSU award to partially fund the purchase of a special wire saw for cutting and preparing optical crystals with exceptionally low strain or deformation and with high precision. This wire saw has unique capabilities beyond anything achievable with a traditional blade saw that are required for preparation of optical samples for photonic research and applications where minimizing residual crystal stress can be critical. Research on this MREDI effort will greatly benefit from the capability to produce precise thin samples with parallel surfaces. Currently, such samples cannot be produced locally and cost several thousands of dollars each when prepared by outside vendors. This sawing system provides much needed infrastructure for long-term research and development, enabling fabrication of small low-strain optical samples for photonics and quantum information projects (reduced crystal defects, precise crystallographic orientation, study of highly absorbing materials, etc.). This capability provides new collaborative R&D funding opportunities with local optics companies, including Scientific Materials Corp (e.g. thin samples for radiation detectors), AdvR Inc (e.g. precision wafers for strip-loaded optical waveguides), and S2 Corp (e.g. thin crystals with large surface area for heat extraction).

- In consultation with MSU Spectrum Lab, S2 Corporation contracted the growth of a Tm:$LiNbO_3$ crystal from United Crystals with S2 internal funds to explore potential vendors of bulk $LiNbO_3$ material and to compare with materials grown in Montana by Scientific Materials Corp. Samples were provided to S2 Corporation, but upon inspection were shown to have significant optical scattering and in one sample large refractive effects. Further evaluations and discussion with United Crystals are in progress.

- Outreach to local Montana schools to promote science, technology, engineering, and mathematics (STEM) was carried out by MREDI-supported graduate student Tino Woodburn during this quarter. This volunteer work involved presentations, discussions, and science activities with school children at Mindbenders Preschool at the Lone Mountain Gym in Bozeman (May 17 & 18, and June 7 & 8).

- Undergradute student Kyle Olson volunteered once a week at Eagle Mount, a local Bozeman non-profit foundation helping those with disabilities. The program pairs volunteers with special needs children and adults to teach them how to rock climb indoors, as well as build relationships and help each other grow.

- The Cone Group has designed and developed a new sample mount apparatus to hold optical crystals within the Montana Instruments Cryostation system. Machining and design was done by graduate student Aaron Marsh in the MSU Physics department machine shop and specialized electroplating to improve thermal shielding was carried out by Dr. Charles Thiel and Tino Woodburn. The rapid development of the new sample holder demonstrates the ease of adapting the Montana Instruments Cryostation to specific applications, and has directly expanded the MSU research capabilities.

- Material characterization in collaboration with Scientific Materials Corp.: Graduate students Aaron Marsh and Tino Woodburn worked with Scientific Materials Corp to gain expertise in using Scientific Materials' Laue x-ray diffraction instrument to determine the orientation of the microscopic crystal structure and then fabricate samples with the lattice structure oriented in along precisely controlled directions (outlined in Figure). This work also helped us to interpret electron backscatter diffraction data acquired in measurements with the FE-SEM and the new Nano-Auger instrument at MSU ICAL.

Advice on polishing crystals has also been exchanged between our lab and Scientific Materials with both parties have benefitting in productivity and quality of results.

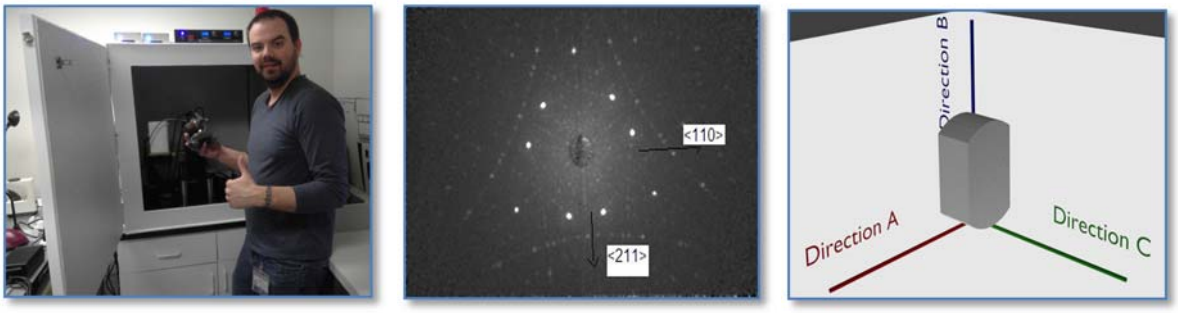

Figure 39. (left) Scientific Materials Corp personnel assisting MSU students with using the company's Laue x-ray diffraction system to probe the atomic structure of their samples. (center) Example pattern of x-rays diffracted from atoms in the crystal, providing information on the structure and orientation of the crystal lattice. (right) Orientation of the crystal axes of a sample from the measured diffraction pattern.

- Material and waveguide characterization in collaboration with AdvR Inc.: During this quarter, MSU students on the MREDI effort worked closely with AdvR Inc personnel to better characterize optical waveguides. In particular, AdvR provided instruction on waveguide coupling and characterization and also provided access to their M-Line Spectrometer for our students to use on this project; an example of a measurement is shown in Fig. 40. Work also continues on developing our Ellipsometric waveguide characterization techniques in the MSU Cone Lab in the Physics Department.

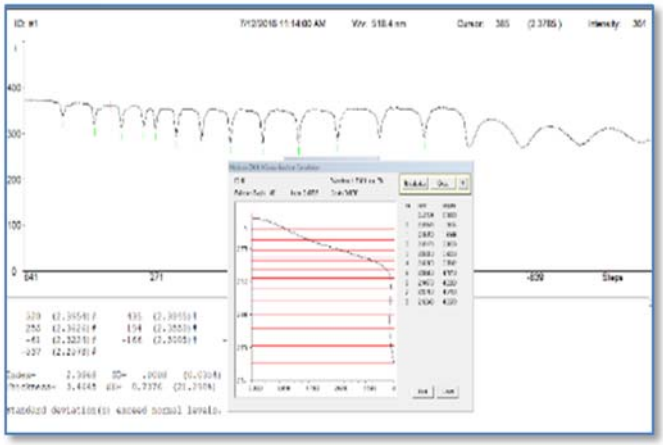

Figure 40. Example M-Line spectrum acquired using AdvR's system, where each peak represents a mode of the optical waveguide. The index profile is modeled in the foreground, though its accuracy for our samples must be verified.

- A technique was developed for measuring the effects of spectral broadening due to vibrations and acceleration in the cryo-cooling cycle of closed cycle cryostats. Two locally produced Montana low vibration cryostats were measured and found to both be "low" vibration systems with respect to vibrational broadening (sub-10 KHz broadening is sufficient for most S2 processors). The vibrational performance of the two cryostat were equal within the systematic errors of the set-ups and measurements. We want to thank Montana Instruments for the loan of their Cryostation, which enabled this testing, as well as the training of two graduate students and an undergraduate student. We also thank S2 Corporation for valuable assistance. The testing performed under this MREDI effort will benefit Montana Instruments and S2 Corporation in their development and marketing of their cryogenic instruments. The knowledge gained about the measurement and behavior of vibrational broadening benefits S2 Corporation in their development of S2 processing devices. The current optical setup with the SHI/S2C system will next be developed into a passive microwave imaging system based on a sensitive broadband S2 correlator. The system may also be used for testing of waveguide devices at cryogenic temperatures.

- As part of the initiative to spur economic development, one of our goals is to enable new optical crystals designed by MSU to be produced by *Scientific Materials FLIR* (Bozeman, MT), a company that specializes in the growth of high-quality crystalline materials for lasers and other related opto-electronic technologies. As part of this, MSU has been working with Scientific Materials on this MREDI effort to develop a series of new crystal growths for materials that are leading commercial products in the opto-electronic market. During this quarter, several new rare-earth-activated lithium niobate crystals were grown at Scientific Materials, leading to several new insights into potential improvements and modifications of their growth procedures and systems to further improve their results. In addition, materials activated by other chemical constituents that improve resistance to optical damage are continuing to being developed and studied under this effort, such as magnesium-doped lithium niobate, with direct impact on our specific project goals as well as being expected to lead to new Montana products for Scientific Materials. In addition, the high consistency and quality of the materials produced by Scientific Materials are being studied at MSU to understand how the material quality may be even further engineered to meet specific needs of different optical applications.

Expenditures to date (Grant 41W416) Personnel $144,541.89 Benefits $35,796.89 Operations $90,179.96, Capital Equipment $122,200. Total Expenditures **$392,718.80.**

Subproject 9: Optical Parametric Oscillator for Tunable Lasers (Kevin Repasky, repasky@ece.montana.edu, with AdvR, Inc.). Investigate optical parametric oscillator performance in support of characterizing large aperture periodically poled non-linear optical crystals and in support of continued development of large area methane detection.

Milestones

a) December 2016: Model optical parametric oscillator performance using SNLO modeling tools
b) June 30, 2017: Demonstrate singly resonant optical parametric oscillator pumped at 1064 nm and seeded at 1650 nm
c) June 30, 2017: Final report including scientific merit and commercial products or potential

Progress toward objectives

Some adjustments were made to the OPG/OPA setup due to the limitation on the commercially available mirrors for building the OPO. The final setup for an OPG/OPA/OPO is completed with a schematic shown in figure 41. As in the previous setup, a 10 ns pulsed laser with 1064 nm wavelength (shown with the green line) is used as a pump source. A CW DFB laser at a wavelength of 1571 nm, amplified through an optical amplifier, is used as a seed laser (shown with the red line). A half wave plate and a polarizer are used for controlling the laser energy without changing its Gaussian beam properties. A dichroic mirror is used to combine both beams and make them collinear. A magnesium-doped lithium niobate crystal is used in the nonlinear process. Two Pellin-Broca prisms are used to separate the spectrum. In the new setup, the crystal and all of the optic components after the crystal are moved further away in order to fit the optical cavity into the system. Additionally, the third focusing lens is replaced from a 500 mm to a 400 mm focal length lens. The transmission through each section is also measured and indicated in the schematic.

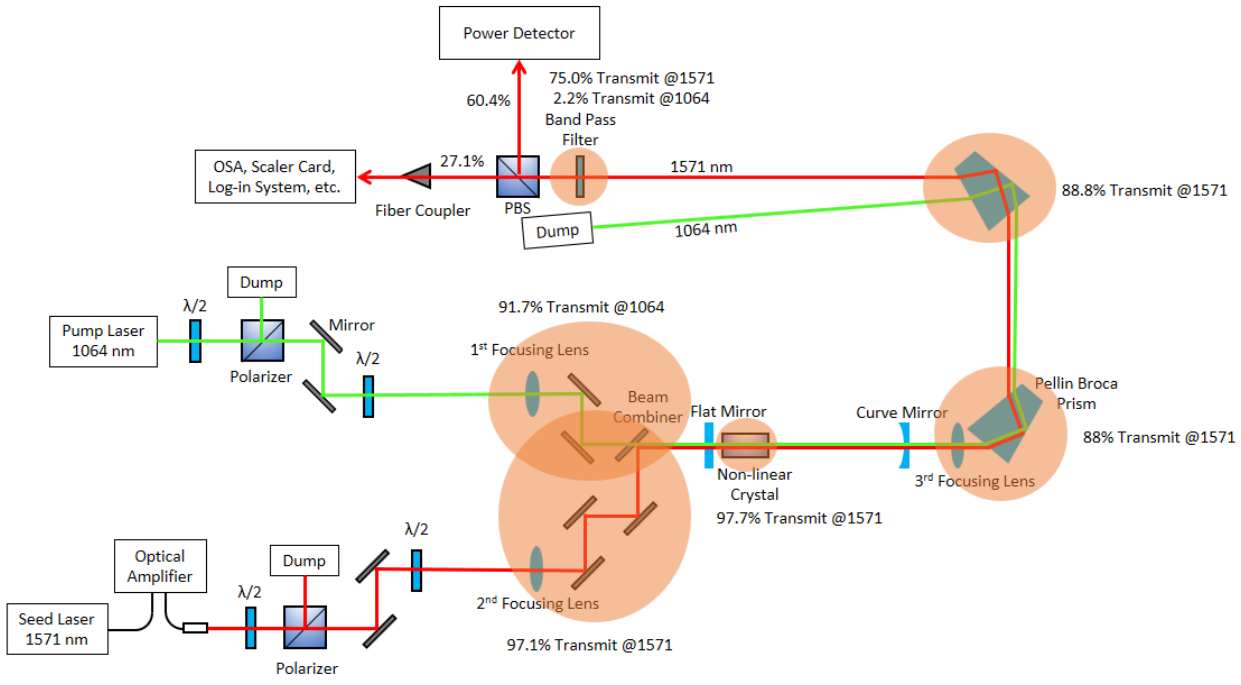

Figure 41. Schematic of the setup for the OPO laser.

In the design, both the pump and the seed beam's position and size were carefully measured. The Gaussian fit of the beams and their properties were acquired from a custom Matlab program as shown in figure 42. The crystal represented as a black box is placed at a location shown in the figure. Based on the availability of the mirror's radius of curvature and reflectivity, the optical resonator is designed to be a hemispherical type using a flat-concave 99%-50% reflectivity at 1550 nm. The flat mirror is measured to have a reflectivity of 98.8% at 1571 nm and 23.8% at 1064 nm. The concave mirror is measured to have a reflectivity of 45.7% at 1571 nm and 21.1% at 1064 nm.

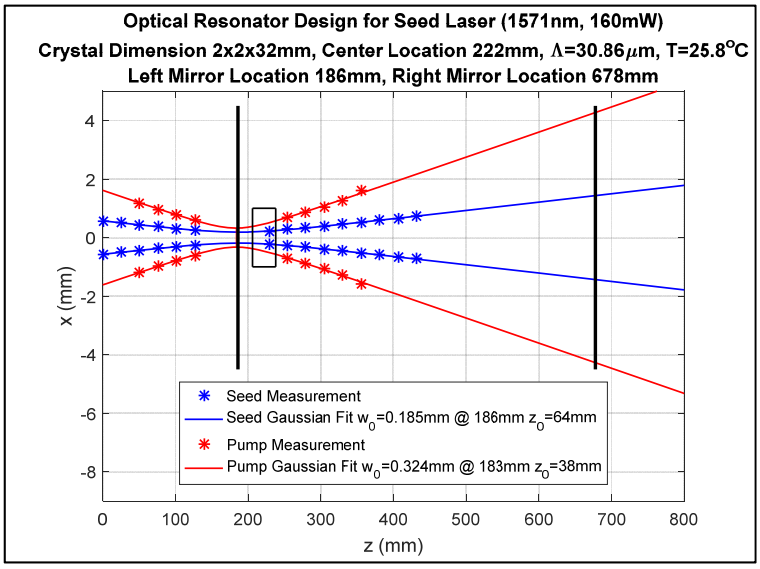

Figure 42. Pump and seed beam sizes for the optical resonator design.

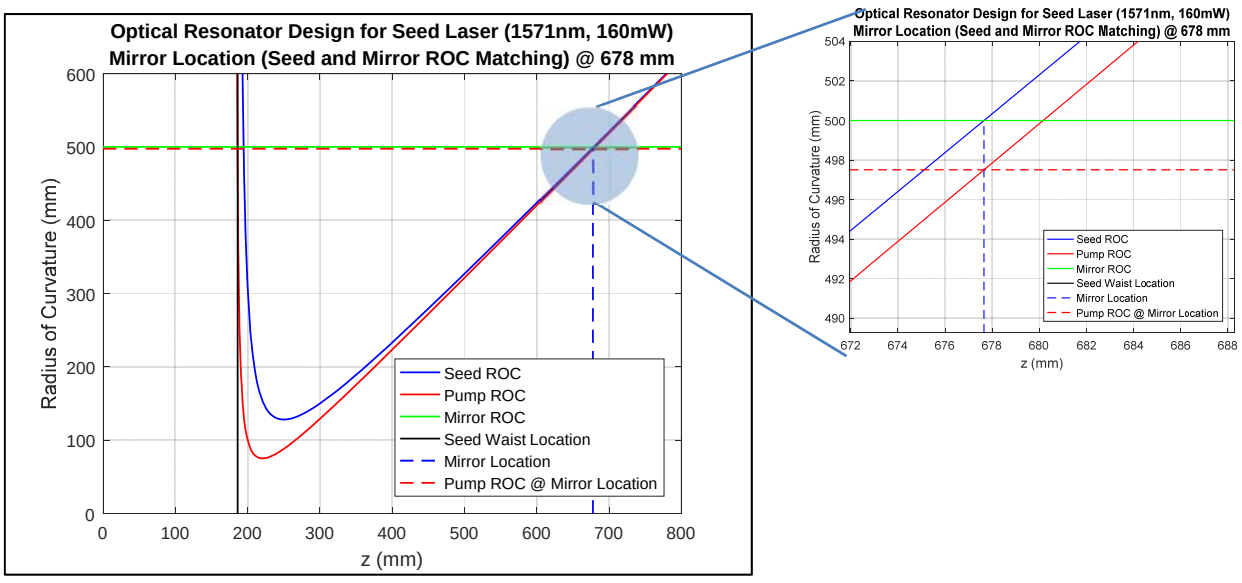

Figure 43. Radius of curvature of the seed and pump beams for the optical resonator design.

For best results, both mirrors are placed where their radius of curvature matches that of the seed beam. The flat mirror (the left black line in Fig. 42) is located at the waist location of the seed beam where the radius of curvature is infinity. Figure 43 shows the matching between the concave mirror and the seed beam's radius of curvature. In the figure, the radius of curvature of the seed beam is plotted in blue where its waist location is shown with the black vertical line. The location to place the concave mirror is determined from the interception between the blue curve and the horizontal green line that represents the radius of curvature of the mirror of 0.5 m. From Figures 42 and 43, the beam size and the radius of curvature of both the pump and seed beams at the crystal face, flat mirror, and concave mirror are also calculated as they are needed for the input in the SNLO model. As an example, the radius of curvature of the pump beam at the concave mirror surface is determined from the interception between the vertical dash blue line (where the mirror is placed) and the red curve (pump radius of curvature) as shown in the zoomed in region of Fig. 43.

To align the optical resonator, the flat mirror is attached to a PZT which is controlled by a ramp generator. Similar to a scanning Fabry-Perot, the PZT voltage is ramped by a saw-tooth function to scan through the cavity lengths where the seed laser can be transmitted. By doing so, the cavity can be aligned for the seed wavelength and the coupling can be optimized. The optimized response of the output frequencies from the cavity detected by an InGaAs detector is plotted in an oscilloscope as shown in Fig. 44. From the ratio between the FSR and FWHM shown in Fig. 45, the measured finesse from these peaks is determined to be 7.04 whereas the calculated finesse from the mirrors' reflectivity is 7.85. Note that the best finesse ever achieved so far in this experiment is about 7.40.

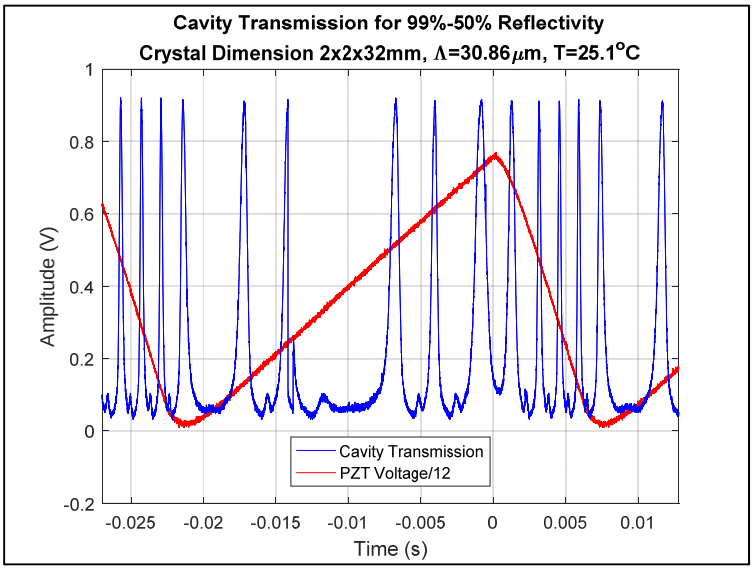

Figure 44. Cavity transmission for 99%-50% reflectivity mirrors.

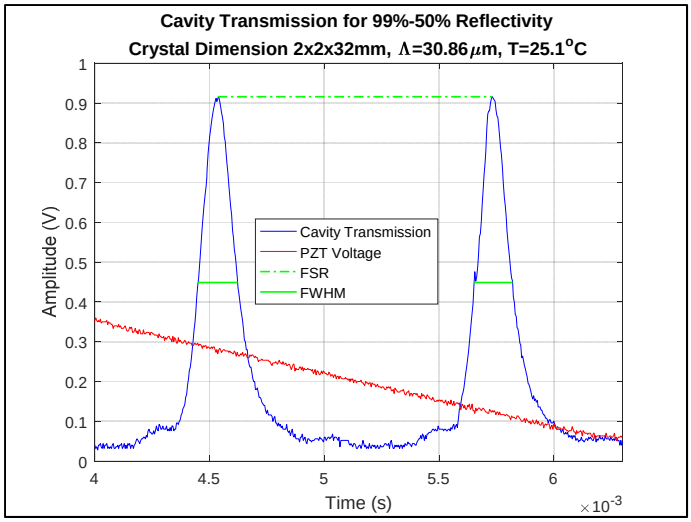

Figure 45. Zoom in of the cavity transmission for 99%-50% reflectivity mirrors.

The output signal energy of the OPG/OPA was carefully re-measured under the same circumstances (except for having the optical cavity in place) as the unseeded-unlocked and seeded-unlocked OPO. Besides allowing more space for adding an optical cavity into the system, another big improvement of the new setup is the accuracy on the measurement of the output signal energy at 1571 nm. The extended distance from prism 1 to the band pass filter shown in Fig. 41 helps to increase the spreading between the signal and the pump beam. The iris is also added in front of the filter to help block the pump beam. In addition, a black box with a tube shown in Fig. 46 is used to shield the detector from any scattered pump beam from walls inside the lab. The only entrance into the box is through the iris and the filter. Even a small amount of the scattered pump beam can easily ruin the signal measurement because the pump energy is relatively very high compare to the signal energy.

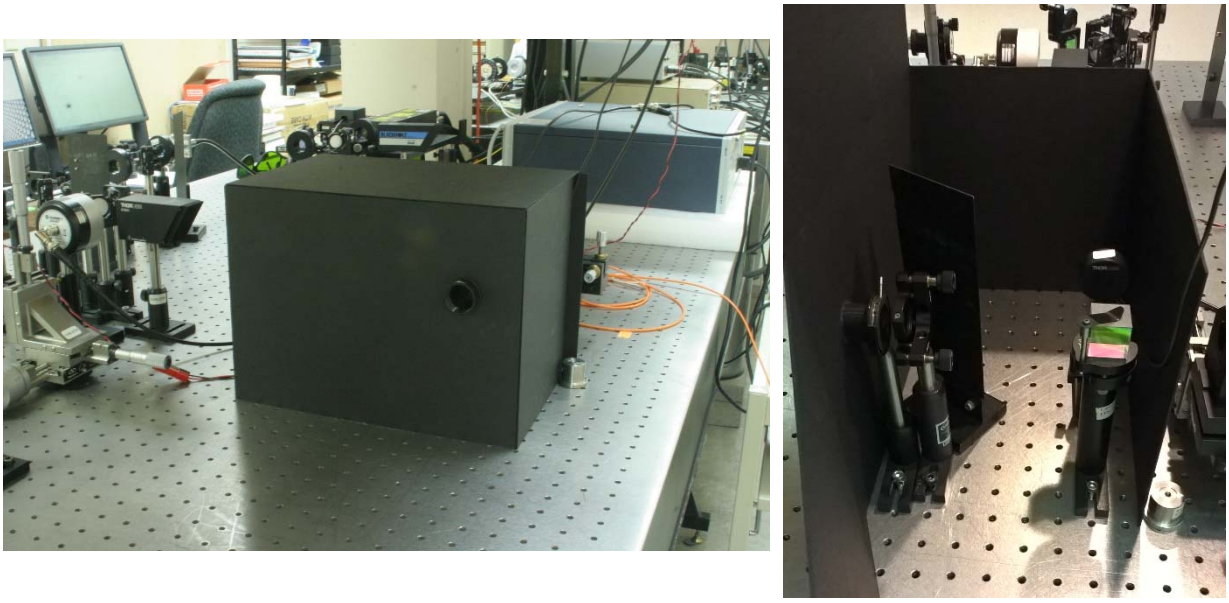

Figure 46. Outside and inside of the black box used for shielding the detector from the pump beam.

Figure 47 shows the results of the output signal energy measurement from an OPG/OPA/unseeded-unlocked OPO/seeded-unlocked OPO case. The output energy from the seeded-unlocked OPO is the highest among the four, followed by the unseeded unlocked OPO, OPA, and OPG as expected. The conversion efficiency for each case is calculated and plotted in Fig. 48.

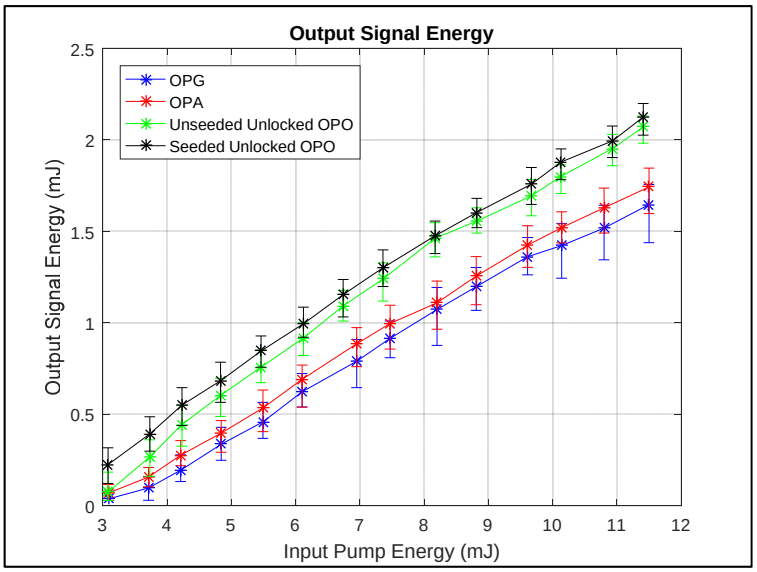

Figure 47. Output signal energy for OPG/OPA/OPO cases.

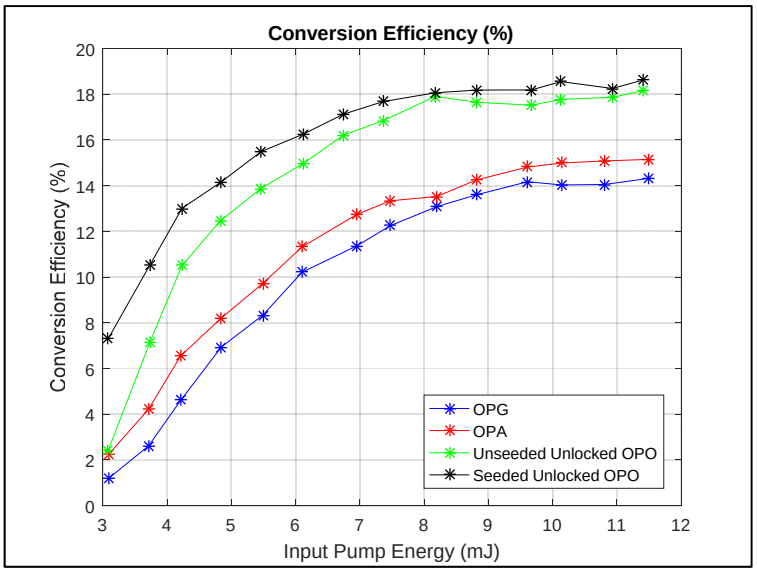

Figure 48. Conversion efficiency correspond to figure 7.

OPG output spectra at several input pump energies are shown in Fig. 49. The spectra get broader and its peak gets higher when the input pump energy increases.

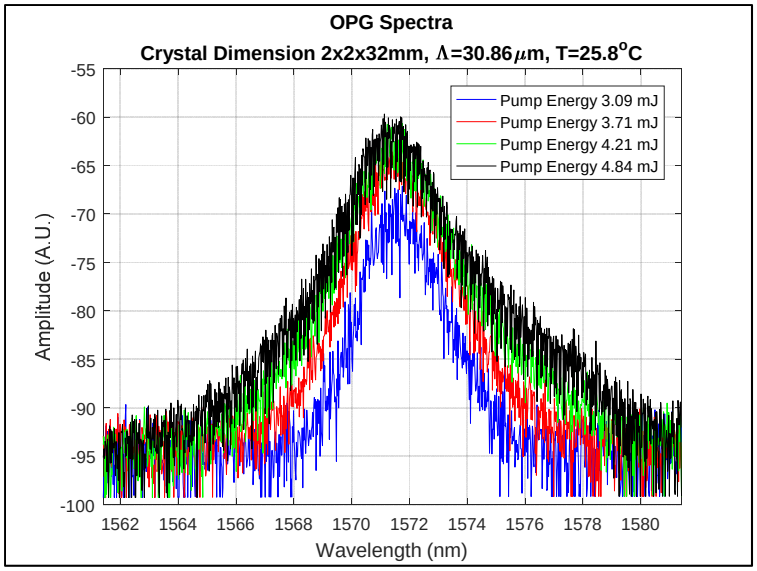

Figure 49. Output spectra for OPG.

OPA output spectra at several input pump energies are shown in Fig. 50. When the input pump energy increases, the base of the spectra broaden while the central peaks remain narrow. This is due to the substantial amount of the laser power being seeded into the crystal.

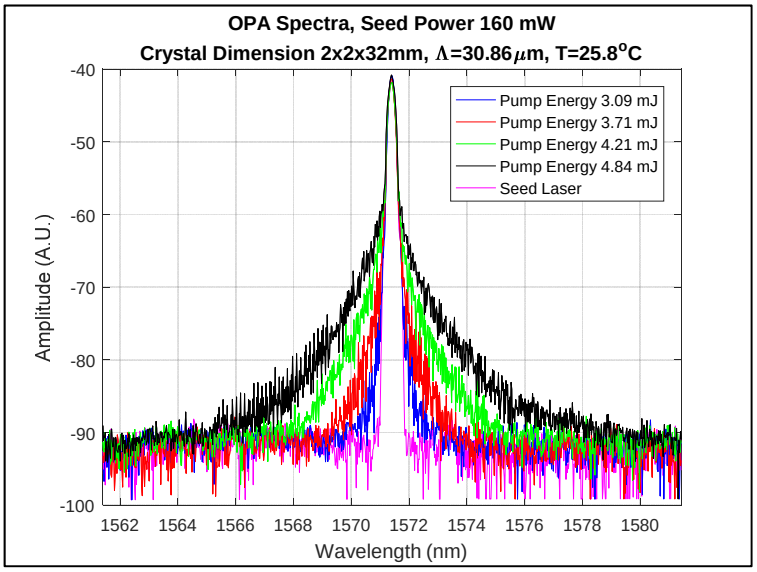

Figure 50. Output spectra for OPA.

Figures 51 and 52 show the comparison between OPG and OPA output spectra for low and high input pump energy. Both cases demonstrate good spectral overlap because the peak of the OPG output spectrum (blue) coincides with the peak of the seed laser spectrum (green), resulting in a narrow OPA output spectrum (red). Both cases also demonstrate good spatial overlap between the seed and pump laser. This overlap can be seen by the narrower base of the OPA output spectrum (red) and the wider base of the OPG output spectrum (blue). If there had been poor spatial overlap, the output OPA spectrum would have broadened so that it would have been nearly as broad as the OPG spectrum.

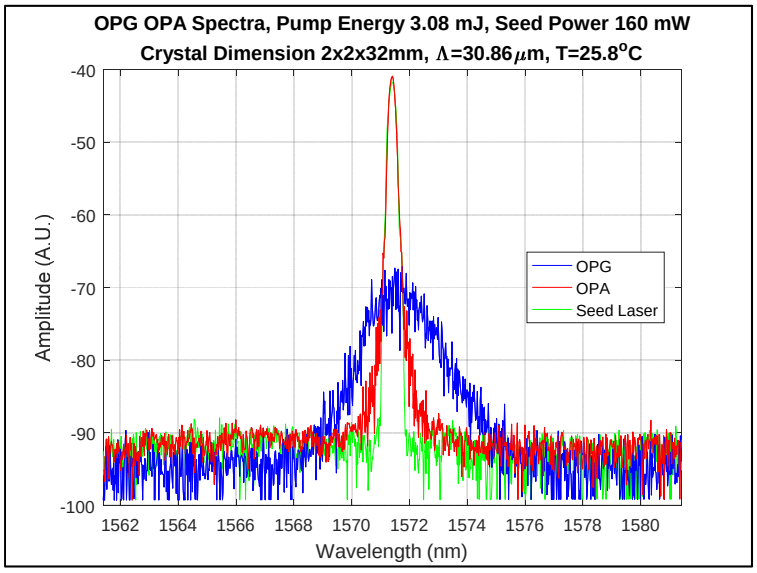

Figure 51. Output spectra for OPG/OPA at low input pump energy.

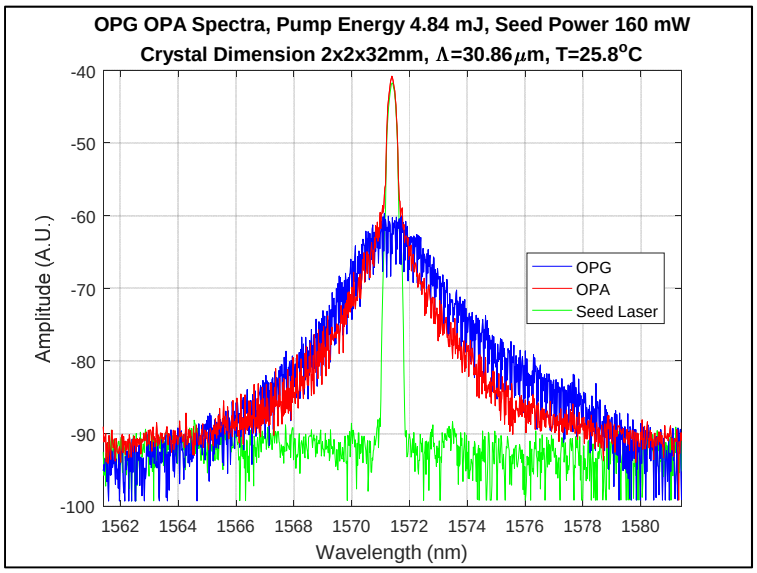

Figure 52. Output spectra for OPG/OPA at high input pump energy.

Figure 53 shows the comparison between the seeded-unlocked and unseeded-unlocked OPO at low and high input pump energy. In both low and high input pump energy cases, the seeded OPO has narrower spectrum than the unseeded OPO overlap (red narrower than blue and black narrower than green), showing good spatial overlap. Both cases also demonstrate good spectral overlap because the peak of the unseeded OPO spectrum coincides with the peak of the seed laser spectrum (blue and green coincide with pink). Notice how the peak of the seeded OPO is narrower at the center than the unseeded OPO, but is still broad (compare to OPA in Figs. 50, 51, and 52) because the cavity is not locked and therefore the cavity length can change due to temperature fluctuations and driven PZT.

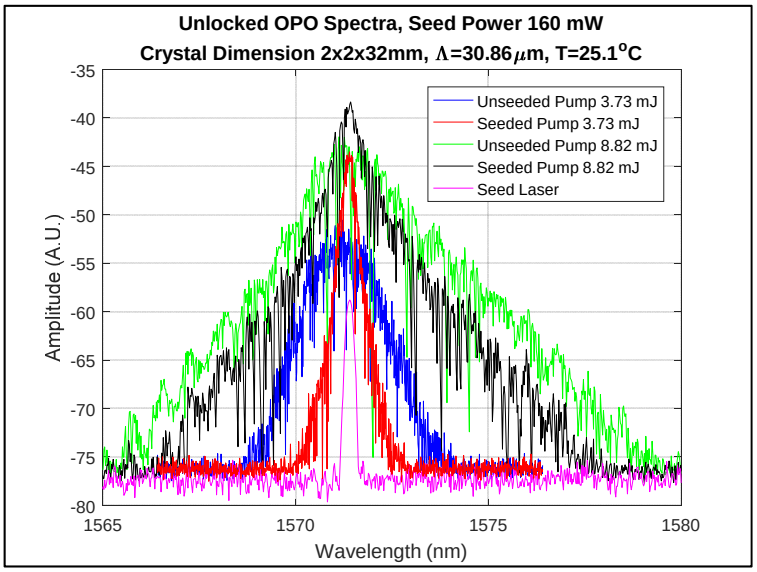

Figure 53. Output spectra for unlocked OPO.

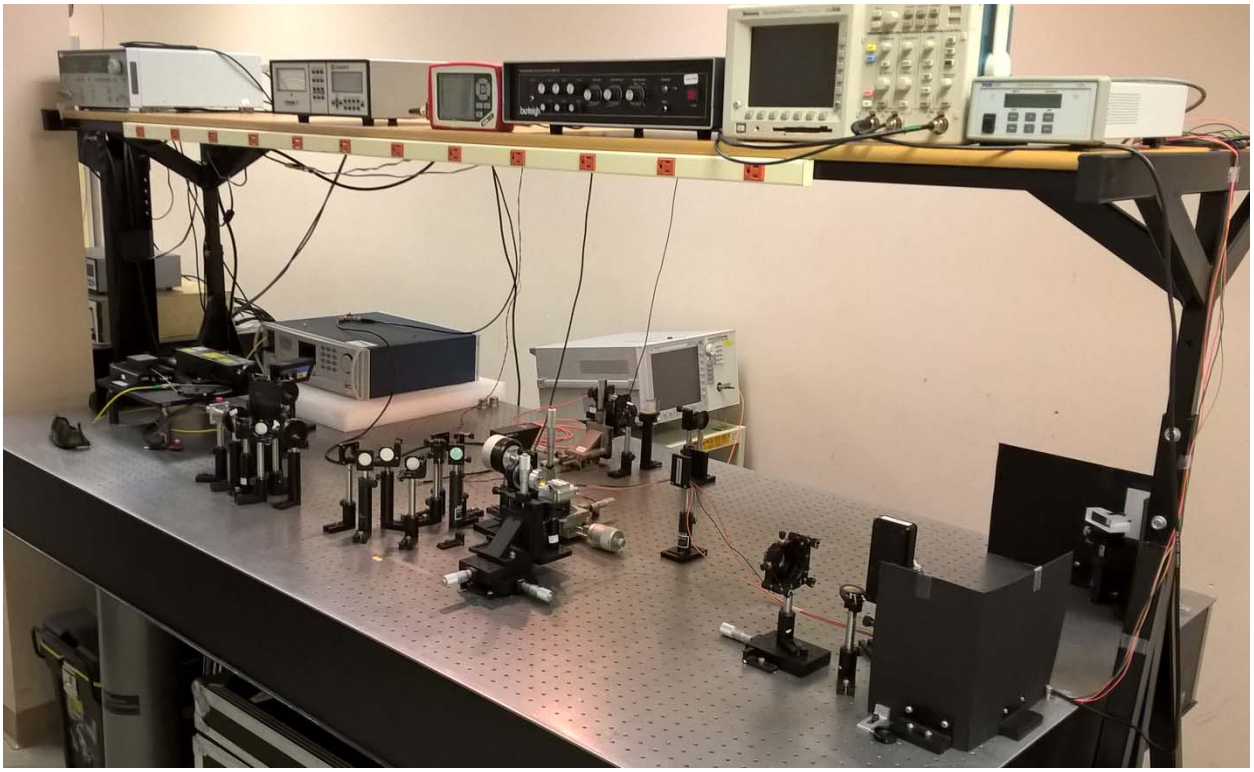

Figure 54. The final OPG/OPA/OPO setup.

Work next quarter will focus on completing the locking setup needed to ensure the seed laser is resonant with the optical cavity. Once this locking is complete, packaging the laser transmitter, shown in Fig. 54, will begin.

Expenditures to date (Grant 41W412) Personnel $34,685.55 Benefits $3,111.40 Operations $22,076.01 total Expenditures **$59,872.96**

Subproject 10: Nonlinear Optical Detection of Surface Contaminants (Rob Walker, rawalker@chemistry.montana.edu, with Altos Photonics). Develop a new method for detecting organic contaminants that accumulate on the surface of water based on nonlinear vibrational overtone spectroscopy (NVOS).

Milestones

a) December 2015: Demonstrate feasibility of using new spectroscopic method for surface detection of adsorbed species
b) June 2016: Submit SBIR application with Altos to develop detection and monitoring instrument based on NVOS
c) December 2016: Successful application of NVOS to environmentally relevant systems including contaminants on water surfaces and solid substrates

Progress toward objectives

This project's goal is to develop new surface specific, optical methods capable of detecting adsorbed molecules. Specifically, our efforts are focused on exploiting the advantages of nonlinear optical spectroscopy to create a simple, sensitive technique that can identify the presence of organic contaminants at water/air and solid/liquid interfaces. Our ultimate objective is to use discoveries from our seminal studies to guide the development of portable devices capable of being used for field measurements.

The second quarter of 2016 started with great promise but we suffered several significant setbacks in June that are likely to cause difficulties for the third quarter of 2016. The difficulties arise from construction for the new dining hall on the north end of CBB. Construction requires extending the steam tunnel from Willson/Jabs and has resulted in large scale excavation and hydraulic pounding. Figure 55 shows the results of an accelerometer app on an i-phone that was placed on a laboratory floor in the basement of CBB (blue trace) and placed on a floating optical table (red).

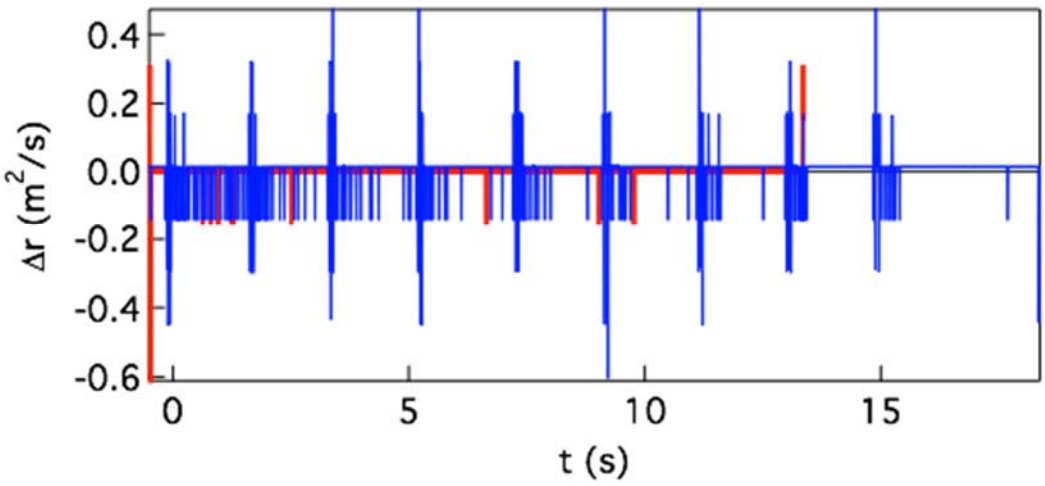

Figure 55. Accelerometer data showing effects of construction-induced vibrations.

The data show the effects of vibrations induced by the construction pounding with a frequency of ~0.7 Hz. The red data show only mild responses that are not correlated with the large amplitude motion measured on the floor.

This disruption leads to visible jitter in the laser beams on the table and ruins alignment in the Ti:sapphire amplifier. Furthermore, the disturbance also ruins alignment in the optical parametric amplifier intended to produce the near infra-red light needed for the planned experiments. The output from the Ti:sapphire laser drops by ~20% following one of these 'pounding' events (duration ~30-60 sec) and the OPA power drops by more than a factor of 2 (190 mW of ω_{idler} power at 1770 nm to 81 mW).

The construction is anticipated to continue well into the Fall '17 semester. Our laboratory does not have a floating optical table. (The table used to make all of the accelerometer measurements was located in the Grumstrup lab, also in the basement of CBB.) The Grumstrup Lab does have an empty 4 x 12 floating table currently not in use. One solution to our current difficulties is to disassemble our NLO spectrometer and reconstruct it on the unused table in the Grumstrup lab. Doing so will require another service visit from Coherent and still require an additional month of rebuilding the experiment. We are currently negotiating with University Administration to cover the costs of this unanticipated expense.

Prior to the start of dining hall construction, the NLO spectrometer was working well and providing very encouraging results. In April and May, we had begun acquiring the benchmark spectra necessary to test the hypothesis that vibrational overtones could be used to generate surface specific, second order nonlinear optical data.

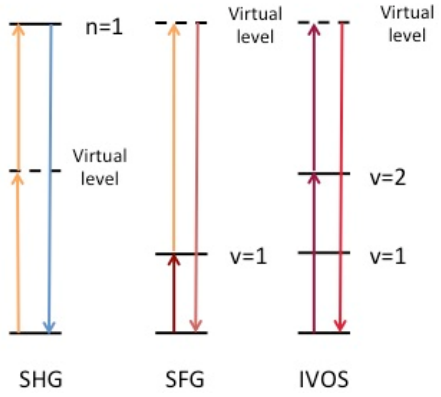

Figure 56: Energy level diagrams for relevant non-linear optical spectroscopies

The proposed NLO methods to be developed in this project build off of conventional surface specific, 2nd order NLO (or $\chi^{(2)}$) techniques. Second order NLO spectroscopies, including second harmonic generation (SHG) and sum frequency generation (SFG), are techniques used to investigate the behavior of molecules at interfaces. Due to their inherent selectivity for the molecules at the surface, they allow detection of spectroscopic signatures from molecules influenced by surface anisotropy without interference from the molecules that make up the isotropic bulk materials on either side of the interface. However, the interfaces that can be examined by these techniques are limited by the need for complicated instrumental set-ups and, in the case of buried interfaces between two condensed phases, the limited transparency of many bulk materials in the visible and infrared (IR) regions of the electromagnetic spectrum, where SFG and SHG provide the most information. (Figure 56) SHG uses two incident photons of frequency ω to generate a single resultant second harmonic SH photon of frequency 2ω, and is typically performed with incident photons in the visible region, generating photons in the ultraviolet. When either the incident or the generated second harmonic light is resonant with an electronic transition of the interfacial molecules, the SH signal experiences a large resonant enhancement, making SHG well-suited to study the electronic structure of interfacial molecules and materials.

SFG is similar in principle to SHG. In SFG, 2 photons of frequencies ω_1 and ω_2 combine to give a single photon of frequency ω_3, where $\omega_3 = \omega_1 + \omega_2$. A typical SFG experiment uses incident beams in the visible and infrared (IR) regions to generate a sum frequency (SF) photon. When the IR frequency is resonant with a vibrational transition of the interfacial molecules, enhancement of the SF signal will occur, allowing detailed structural information about the interfacial molecules to be gathered. SFG requires that 2 pulsed laser beams overlap at the sample in both time and space, as well as necessitating that at least one medium making up the interface be transparent to both visible and IR light. These technical constraints limit the utility of SFG when studying buried interfaces.

In April, we were able to calibrate the wavelengths being generated by the OPA. To do that, a nonresonant SFG spectrum was acquired from a gold surface and then the same spectrum was reacquired only with a polystyrene film in the IR path. Polystyrene has a very distinctive IR absorption spectrum, so any sum frequency response from the Au surface would be attenuated at frequencies corresponding to the polystyrene vibrational modes. Figure 57 shows SFG spectra acquired from Au and Au with polystyrene in the optical path. Superimposed on these data is the simple IR absorption spectrum of polystyrene itself.

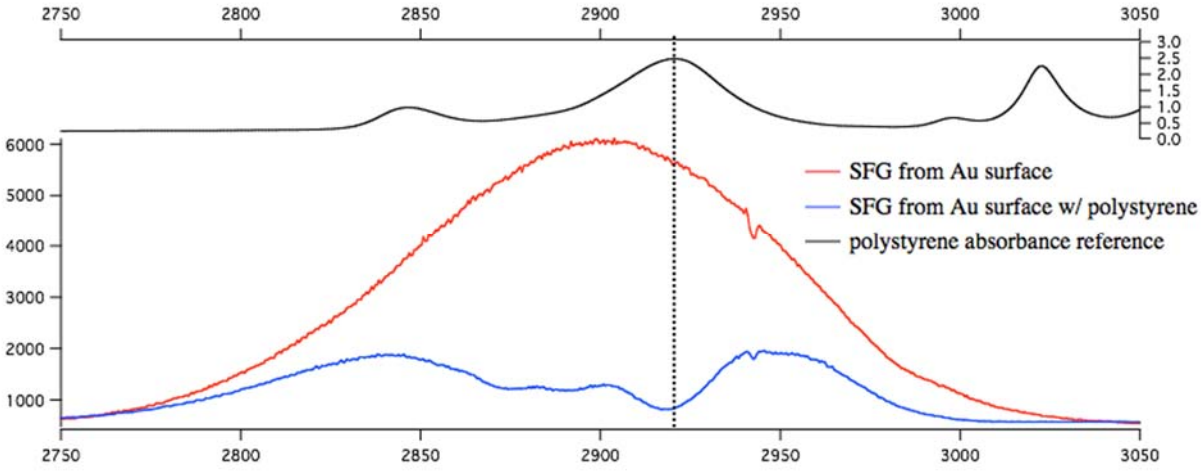

Figure 57. SFG spectra acquired from Au and Au with polystyrene in the optical path.

These data are revealing. First, they show us that the SF light being generated is not being distributed uniformly across the CCD. (If we had uniform distribution, the polystyrene peaks would match the divots in the SFG spectrum (in blue).) Second, we observed that the PS calibration leads to significant attenuation overall of the observed SFG signal from the Au substrate.

To correct these problem, we reoptimized the system's collection optics and narrowed the resolution of the 800 nm light being used to upconvert the IR signal and create the SF response. The results were striking as evidenced by the SFG spectrum acquired from the air/vapor interface of dimethyl sulfoxide (DMSO) shown in Fig. 58.

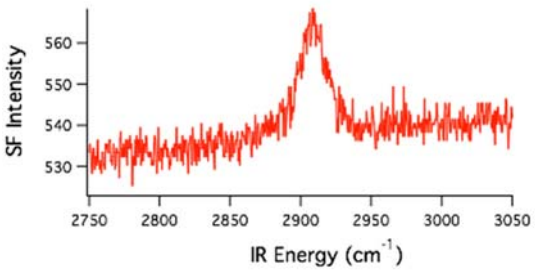

Figure 58. SFG spectrum from air/vapor interface of dimethyl sulfoxide (DMSO).

We also then acquired an SFG response from a Au surface covered with a covalently bound octadecanethiol monolayer. In this experiment, the vibrational resonances from the thiol monolayer are 180˚ out of phase from the nonresonant response of Au, thus the vibrational SFG resonances appear as negative going peaks in the Au spectrum. The results are shown in Fig. 59.

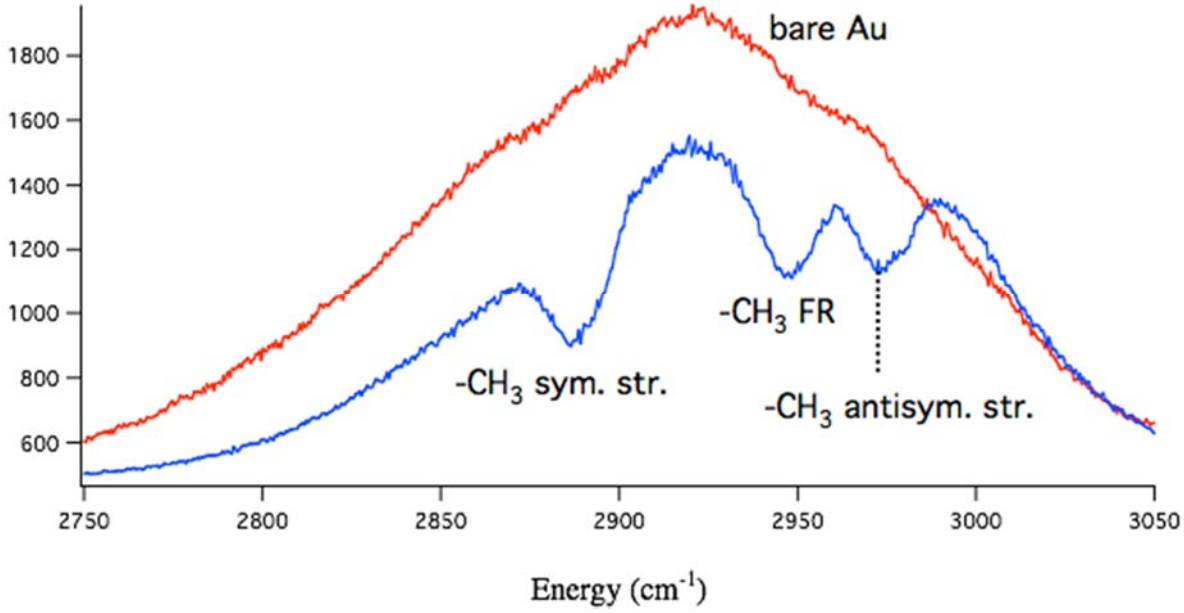

Figure 59. SFG response from Au surface covered with covalently bound octadecanethiol monolayer.

In this figure, the methyl symmetric stretch (-CH_3 sym. str. at 2880 cm^{-1}) and Fermi Resonance (CH_3-FR at 2940 cm^{-1}) are indicative of a highly ordered array of alkyl chains tilted ~20˚ off of surface normal.

The next step in this progression was to perform experiments using ω_{idler} and try to observe an SFG response from the overtones of the methyl symmetric stretch, but this timing coincided with the start of construction.

In Q5, we will begin moving our NLO assembly from its current location to an empty floating table in the Grumstrup lab in the hopes of being able to again perform experiments without the disruption from

construction activity. Given the intransigence on the part of university administration to assist us in a timely fashion, it is difficult to anticipate how quickly or slowly this will go.

A brighter development is that a white paper submitted to ARO has been invited for full proposal submission (due September 1). If successful, that award will put this work on secure financial footing.

Expenditures to date (Grant 41W415) Personnel $16,985.93 Benefits $1199.60 Operations $16,038.88., total Expenditures **$34,224.41.**